The global gas and dust budget of the Large Magellanic Cloud: AGB stars and supernovae, and the impact on the ISM evolution

M. Matsuura[1,2], M.J. Barlow[2], A.A. Zijlstra[3], P.A. Whitelock[4,5,6], M.-R.L. Cioni[7], M.A.T. Groenewegen[8], K. Volk[9], F. Kemper[3], T. Kodama[1], E. Lagadec[3], M. Meixner[10], G.C. Sloan[11], S. Srinivasan[12],

[1] *National Astronomical Observatory of Japan, Osawa 2-21-1, Mitaka, Tokyo 181-8588, Japan*
[2] *Department of Physics and Astronomy, University College London, Gower Street, London WC1E 6BT, United Kingdom*
[3] *Jodrell Bank Centre for Astrophysics, School of Physics and Astronomy, University of Manchester, Oxford Street, Manchester M13 9PL, United Kingdom*
[4] *South African Astronomical Observatory, P.O.Box 9, 7935 Observatory, South Africa*
[5] *NASSP, Astronomy Department, University of Cape Town, 7701 Rondebosch, South Africa*
[6] *Department of Mathematics and Applied Mathematics, University of Cape Town, 7701 Rondebosch, South Africa*
[7] *Centre for Astrophysics Research, University of Hertfordshire, Hatfield AL10 9AB, United Kingdom*
[8] *Royal Observatory of Belgium, Ringlaan 3, B-1180 Brussels, Belgium*
[9] *Gemini Observatory, Hilo, HI, USA*
[10] *Space Telescope Science Institute, 3700 San Martin Drive, Baltimore, MD 21218, USA*
[11] *Astronomy Department, Cornell University, 610 Space Sciences Building, Ithaca, NY 14853-6801, USA*
[12] *Department of Physics and Astronomy, Johns Hopkins University, Homewood Campus, Baltimore, MD 21218, USA*

ABSTRACT

We report on an analysis of the gas and dust budget in the the interstellar medium (ISM) of the Large Magellanic Cloud (LMC). Recent observations from the *Spitzer Space Telescope* enable us to study the mid-infrared dust excess of asymptotic giant branch (AGB) stars in the LMC. This is the first time we can quantitatively assess the gas and dust input from AGB stars over a complete galaxy, fully based on observations. The integrated mass-loss rate over all intermediate and high mass-loss rate carbon-rich AGB candidates in the LMC is $8.5 \times 10^{-3} \, M_\odot \, \mathrm{yr}^{-1}$, up to $2.1 \times 10^{-2} \, M_\odot \, \mathrm{yr}^{-1}$. This number could be increased up to $2.7 \times 10^{-2} \, M_\odot \, \mathrm{yr}^{-1}$ if oxygen-rich stars are included. This is overall consistent with theoretical expectations, considering the star formation rate when these low- and intermediate-mass stars where formed, and the initial mass functions.

AGB stars are one of the most important gas sources in the LMC, with supernovae (SNe), which produces about 2–$4 \times 10^{-2} \, M_\odot \, \mathrm{yr}^{-1}$. At the moment, the star formation rate exceeds the gas feedback from AGB stars and SNe in the LMC, and the current star formation depends on gas already present in the ISM. This suggests that as the gas in the ISM is exhausted, the star formation rate will eventually decline in the LMC, unless gas is supplied externally.

Our estimates suggest 'a missing dust-mass problem' in the LMC, which is similarly found in high-z galaxies: the accumulated dust mass from AGB stars and possibly SNe over the dust life time (400–800 Myrs) is significant less than the dust mass in the ISM. Another dust source is required, possibly related to star-forming regions.

Key words: galaxies: evolution – galaxies: individual: the Magellanic Clouds – (ISM:) dust, extinction – stars: AGB and post-AGB – stars:mass-loss – (stars:) supernovae: general

1   INTRODUCTION

The interstellar medium (ISM) of a galaxy is one of the drivers of its evolution, and the composition of the ISM determines many of the characteristics of the next generation of stars. The ISM is itself continuously renewed and enriched by stellar ejecta. The enrichment occurs as stars evolve and die, either exploding as supernovae (SNe) or experiencing intense mass loss in a super-wind. Super-winds occur in low and intermediate mass stars during the asymptotic giant branch (AGB) phase (main sequence masses in the approximate range 1–$8\,M_\odot$), and in more massive red supergiants. The ejecta are enriched with elements produced in various phases of nuclear burning. In general terms, gas ejected from SNe includes newly synthesised heavy elements, such as oxygen, iron and silicon (Nakamura et al. 1999), while AGB stars (below $8\,M_\odot$) synthesize lighter elements, especially carbon and nitrogen (Maeder 1992). The chemical evolution of the gas can be well understood in terms of the different stellar sources (e.g. Chiappini et al. 2001), taking into account the need for infall of unprocessed gas to stabilize the final metallicity (Finlator & Daveé 2008). The chemical evolution of the Large Magellanic Cloud (LMC) has recently been studied by Carrera et al. (2008).

The origin of the dust in the ISM is less well understood. Dust forms in stellar ejecta at temperatures of about 1000–$1500\,\mathrm{K}$ and at high densities. Different stars produce different types of dust. Red supergiants produce oxygen-rich (silicate) dust. AGB stars have two distinct chemical types: oxygen- and carbon-rich, depending on the abundance ratio of oxygen and carbon atoms within their atmospheres. Oxygen-rich stars form silicate dust, while carbon-rich stars yield amorphous carbon, graphite and SiC dust. Supernovae can produce both dust types, depending on the abundances in the different layers of the ejecta (Rho et al. 2008).

The current rate of ISM enrichment by dust and gas depends on the total stellar population, the initial mass function and the star-forming history (e.g. Salpeter 1955). Type II SNe are expected to dominate the enrichment in the early phases of galaxy evolution (e.g. Maeder 1992). Hirashita & Ferrara (2002) argue that dust grains injected from SNe into the ISM accelerate star formation in young galaxies. It takes more than $100\,\mathrm{Myr}$ for the first intermediate-mass stars to evolve onto the AGB (e.g. Vassiliadis & Wood 1993). Thus, dust and gas enrichment from AGB stars occurs later than from high-mass stars. Different galaxies, at different stages of this process, may be expected to show differences in gas-to-dust ratios, dust content, and, in consequence, ISM dust extinction curves.

In our Galaxy, the major dust sources are presumed to be AGB stars and SNe (Gehrz 1989). Some other sources, such as Wolf-Rayet stars and novae, also contribute dust to the ISM of the Milky Way, but only in small quantities (Gehrz 1989). The relative importance of AGB stars and SNe remains uncertain. Dwek (1998) suggests that SNe are important silicate dust sources, while most carbonaceous dust grains are from carbon-rich AGB stars. Jura & Kleinmann (1989) show

that AGB stars are an important gas source within our Galaxy, except in the Galactic plane where SNe appear to dominate. The dust formation efficiency in SNe remains controversial (e.g. Sugerman et al. 2006), since SN shocks also destroy dust (Tielens 1994) and since dust production prior the explosion remains unclear.

There are also uncertainties in the dust formation efficiencies for AGB stars. This is expected to depend on the mass-loss rate, chemical type, and metallicity. For oxygen-rich stars mass-loss rates decrease towards lower metallicity (Wood et al. 1998; Bowen & Willson 1991; Marshall et al. 2004). In contrast, for carbon-rich stars, although the metallicity dependence of mass-loss rates is still unclear (Habing 1996; van Loon 2000; Wachter et al. 2008; Mattsson et al. 2008), there does not appear to be any obvious metallicity dependence in the range from solar, down to one-twentieth of the solar metallicity (Groenewegen et al. 2007; Matsuura et al. 2007; Sloan et al. 2009). However, we would expect the mass-loss rates of carbon stars to differ between environments with different abundances of alpha elements. In these cases the initial abundance of oxygen in the carbon-star precursor would be vital in determining how much carbon must be dredged up before any was free to become dust.

Galaxy evolution models aim at fitting the current composition of the ISM by following the evolution of the stellar population over the lifetime of the galaxy. This requires a detailed knowledge of dust formation efficiencies, gas and dust expulsion efficiencies and nucleosynthesis in stellar interiors. Here we aim to measure the current integrated rate of gas and dust input into the ISM for one specific galaxy: the LMC. Recent observations by the *Spitzer Space Telescope* (hereafter Spitzer (Werner et al. 2004)) facilitate the detection of individual dust formation sites in nearby galaxies. Observations from Spitzer can thus be used to provide a new estimate of the gas and dust budgets for these galaxies.

We have obtained spectra of AGB stars (mainly carbon-rich stars) in the LMC and the Small Magellanic Cloud (SMC) using the Infrared Spectrograph (IRS; Houck et al. 2004) on-board Spitzer (Sloan et al. 2006, 2008; Zijlstra et al. 2006; Matsuura et al. 2006; Wood et al. 2007; Lagadec et al. 2007; Leisenring et al. 2008); there are also independent spectral surveys of these galaxies (Buchanan et al. 2006; Kastner et al. 2008). A complete LMC photometric survey using Spitzer was recently published by Meixner et al. (2006, SAGE). Combining these data we obtain a census of the mass-losing stars, and can then compare AGB stars with other sources of dust and gas in the LMC. The SMC data are not discussed in detail, but are used to extend the colour mass-loss relations to lower mass-loss rates.

2   ANALYSIS

2.1   Mass-loss rates and colours

It has been shown empirically that mass-loss rates of AGB stars correlate with their infrared colours (e.g.
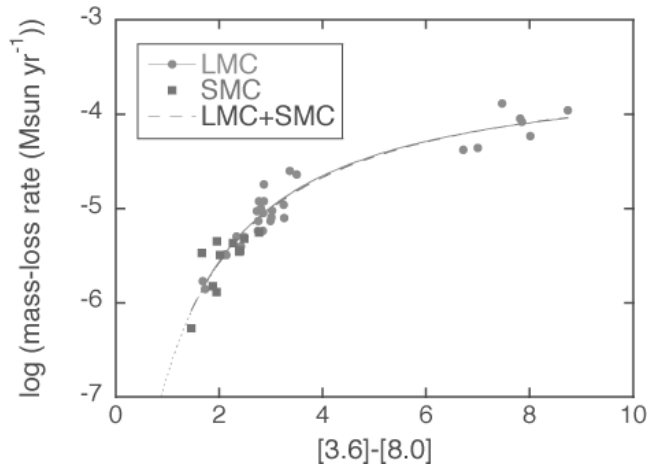
Figure 1. Gas mass-loss rates for LMC and SMC carbon stars from Groenewegen et al. (2007) and Gruendl et al. (2008) are plotted as a function of $[3.6] - [8.0]$ colours extracted from SAGE (Meixner et al. 2006). A gas-to-dust ratio of 200 is adopted. The solid (red) curve is the fit to the LMC sample only and the dashed (green) curve is the fit to the combined LMC and the SMC samples.
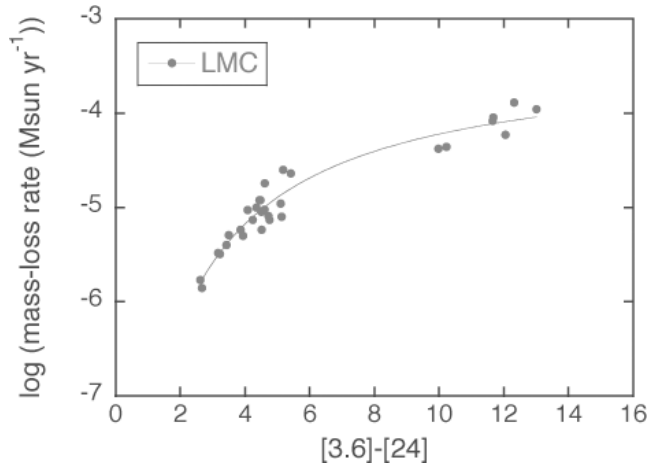

Figure 2. Similar to Fig. 1, showing $[3.6] - [24]$ for the LMC sample.

Figure 3. Similar to Fig. 1, showing $Ks - [8.0]$.

Jura 1987; Whitelock et al. 1994; Le Bertre 1997). Particularly well known is the correlation with $K - [12]$ (Whitelock et al. 2006; van Loon et al. 1999), where [12] is the IRAS $12\,\mu$m magnitude. It is assumed that this arises because K magnitude is a measure of the flux from the central star, while [12] measures the flux from the circumstellar envelope. A similar mass-loss rate versus colour relation has been obtained using $[6.4]-[9.3]$ for carbon-rich AGB stars in the LMC and SMC (Groenewegen et al. 2007). Groenewegen (2006) also provide theoretical relations between mass-loss rates and infrared colours for photometry from Spitzer, 2MASS (Skrutskie et al. 2006) and $AKARI$ (Murakami et al. 2007).

We derive observational mass-loss rate versus colour relations by adopting gas mass-loss rates estimated for carbon-rich AGB stars in the Magellanic Clouds from Groenewegen et al. (2007) and Gruendl et al.
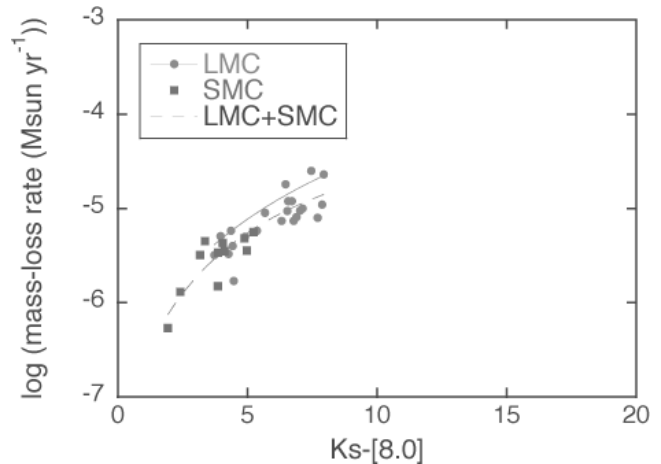
(2008). Groenewegen et al. (2007) used the spectral energy distributions obtained from Spitzer IRS spectra (Sloan et al. 2006; Zijlstra et al. 2006) and $JHKL$ mags observed at Siding Spring Observatory (SSO) in Australia, near simultaneously with the IRS observations (Wood et al. 2007). The spectral energy distributions were fitted using a radiative transfer model. The gas-to-dust ratio is assumed to be 200 for these carbon-rich AGB stars. For all these stars, we extract Spitzer IRAC (Fazio et al. 2004) and MIPS (Rieke et al. 2004) mags. For the LMC the Spitzer and the 2MASS mags are taken from the 2007 version of SAGE (Surveying the Agents of a Galaxy's Evolution; Meixner et al. 2006), while for the SMC they are from S^{3}MC (Bolatto et al. 2007). Stars in clusters are excluded here so as to avoid possible source confusion. We cross-identified for sources within $10\,$arcsec from SAGE and S^{3}MC, using the coordinates quoted in Sloan et al. (2006) and Zijlstra et al. (2006). We found 24 stars in the LMC and 19 in the SMC. Some of them have incomplete photometric data sets from 2MASS and/or SAGE. Highly reddened stars were not detected in the 2MASS J-band. Gruendl et al. (2008) discovered thirteen extremely red objects (EROs) in the LMC, and seven of them were confirmed to be carbon-rich AGB stars, based on IRS spectra; we use their mass-loss rates in the following analysis. Gruendl et al. (2008) measured their magnitudes in the Spitzer IRAC bands and the MIPS 24 and $70\,\mu$m bands, but these stars were not detected in the near-infrared either by 2MASS (Skrutskie et al. 2006) or by Kato et al. (2007).

The average interstellar extinction is estimated to be $E(B - V)$=0.15 and A_{Ks}=0.04 mag towards the LMC and A_{Ks}=0.01 mag towards the SMC (Glass et al. 1999; Zaritsky 1999; Cioni et al. 2006a,b). We can safely ignore the interstellar extinction here, except for the $J - Ks$ versus Ks diagram in Fig. A1, for a comparison with a figure in Cioni et al. (2006a).

Figs. $1 - 3$ show the mass-loss rates as a function of $[3.6]-[8.0]$, $[3.6]-[24]$ and $Ks-[8.0]$, respectively. These relations are fitted with a log function, following Le Bertre & Winters (1998), and the fits are shown in

the figures. Fits to the LMC and SMC combined sample give

$$\log \dot{M}_g = -6.20/(([3.6]-[8.0])+0.83)-3.39 \qquad (1)$$

in the range of $1 < [3.6]-[8.0] < 9$

$$\log \dot{M}_g = -14.50/((Ks-[8.0])+3.86)-3.62 \qquad (2)$$

in the range of $1 < Ks-[8.0] < 9$, and fits to the LMC sample $(3 < [3.6]-[24] < 14)$ give

$$\log \dot{M}_g = -9.89/(([3.6]-[24])+1.43)-3.36 \qquad (3)$$

where $\dot{M}_g$ is the gas mass-loss rate. These equations are fitted for stars with colour ranges of $1.5 < [3.6]-[8.0] < 9$ for eq.(1) $2 < Ks-[8.0] < 8$ mag for eq.(2), $2.5 < [3.6]-[24] < 13$ for eq.(3), respectively. All fits have correlation coefficients higher than 0.8. Coefficients are higher than 0.96 for $[3.6]-[8.0]$ and $[3.6]-[24]$. The photometric data of the EROs contribute to the better fit in the reddest colour range for the Spitzer bands, but these stars were not detected in Ks. MIPS [24] data are used for the LMC only. Relatively low mass-loss rate stars are not detected in MIPS [24] (Fig. A5), and the equation using $[3.6]-[24]$ is suitable for relatively high mass-loss rate stars only. Stars in the SMC sample have bluer infrared colours and lower mass-loss rates than those of the LMC sample; this bias was present in the original sample selection for IRS spectroscopy (Sloan et al. 2006; Zijlstra et al. 2006; Lagadec et al. 2007). If data in all bands are available the equation in $[3.6]-[8.0]$ is the better one for deriving mass-loss rates, except for low mass-loss rate stars, where $Ks-[8.0]$ will be more sensitive to the small dust excess. These two equations will be used later.

These fits should be regarded as very uncertain in the extrapolated regime of extremely low mass-loss rates. Also, the equation fitted for $Ks-[8.0]$ is not appropriate for the mass-loss rates of red carbon stars $(> 10^{-5} M_\odot\,\mathrm{yr}^{-1})$.

Throughout this paper we assume a gas-to-dust ratio of 200 for carbon-rich AGB stars to convert the measured dust mass to a gas mass-loss rate. This ratio is similar to Galactic values (c.f. Habing 1996; Le Bertre 1997; Skinner et al. 1999). Matsuura et al. (2005) argue that, for carbon-rich AGB stars, the gas-to-dust ratio only marginally depends on the metallicity of the host galaxy. This is because carbon atoms are synthesised in AGB stars, and the quantity of amorphous carbon (or graphite) produced depends on the number of excess carbon atoms in the atmosphere of the AGB star after all the oxygen atoms are locked into the stable carbon monoxide molecule. Various observations suggest no obvious differences in mass-loss rates for carbon-rich AGB stars amongst the LMC, the SMC and the Fornax dwarf Spheroidal Galaxy (Groenewegen et al. 2007; Matsuura et al. 2007); the time variations and uncertainties of the mass-loss rates appear to be larger than any metallicity effects. Typical metallicities of the LMC, the SMC, and the Fornax dwarf Spheroidal Galaxy are half, one quarter and one tenth of the solar metallicity, respectively. Theoretical models by Mattsson et al. (2008) and Wachter et al.

(2008) predict that the mass-loss rates should depend on metallicity, although the predicted difference between the LMC and SMC amounts to only a factor of two. Habing (1996) and Matsuura et al. (2007) and argued that the mass-loss rate of carbon stars is primarily determined by the difference in the numbers of carbon and oxygen atoms: as the excess carbon is self produced by the AGB star, carbon stars will show relatively little difference in mass-loss rates between different galaxies, although for low metallicity systems the mass loss may begin earlier on the AGB phase (Lagadec & Zijlstra 2008a). Note that this will apply only to carbon-rich AGB stars; the mass loss of oxygen-rich AGB stars is likely to show a strong metallicity dependence (Wood et al. 1998; Bowen & Willson 1991; van Loon 2000; Lagadec & Zijlstra 2008a).

In the process of estimating the mass-loss rate (Groenewegen et al. 2007; Gruendl et al. 2008), an outflow velocity of the circumstellar envelope is assumed. For oxygen-rich stars, lower outflow velocities are found (Wood et al. 1992; Marshall et al. 2004), but the gas velocity has never measured for carbon-rich stars in the LMC. Theoretical models (Mattsson et al. 2008; Wachter et al. 2008) suggest that the mean velocity does not depend on metallicity for carbon-rich stars. Groenewegen et al. (2007) assumed a gas velocity of $10\,\mathrm{km\,s}^{-1}$, while Gruendl et al. (2008) used 8–$12\,\mathrm{km\,s}^{-1}$.

The other uncertainty originates from the assumption that the dust condensation temperature is $1000\,\mathrm{K}$ (Groenewegen 2006; Gruendl et al. 2008). This is a similar value as used for Galactic stars (Groenewegen 1998). However, for example, the condensation temperature of graphite dust grains varies with carbon-to-oxygen (C/O) ratio (Lodders & Fegley 1995; Tielens et al. 2005), and at a C/O ratio of 1.2, the temperature is $1700\,\mathrm{K}$. It has been suggested that the C/O ratio of carbon-rich stars in the LMC is systematically higher than in their Galactic counterparts (Matsuura et al. 2005, 2006). This has also been suggested from the observations of PNe in the LMC and the SMC (Leisy & Dennefeld 1996; Dopita et al. 1997; Stanghellini et al. 2005). To account for C/O ratio variations and to test their influence of the dust condensation temperature on mass-loss rate, we tested radiative transfer modelling of the SED fitting, with dust condensation temperatured of $1000\,\mathrm{K}$, $1200\,\mathrm{K}$, $1300\,\mathrm{K}$ and $1700\,\mathrm{K}$. We used the spectrum of one of the highest mass-loss rate stars, $050231.49-680535.8$ (J2000), observed by Gruendl et al. (2008). The result shows that both the fitted optical depth and expansion velocity increase with dust condensation temperature. The mass-loss rate required to fit the SED could be a factor of 2.4 higher, if the dust condensation temperature increases from $1000\,\mathrm{K}$ to $1700\,\mathrm{K}$, although the numerical error is large for the models with dust condensation temperature above $1300\,\mathrm{K}$. This suggests that the mass-loss rate, which is estimated from infrared colour, could be underestimated by a factor of up to 2.4, systematically. In the overall analysis, we give the results under the assumption of $1000\,\mathrm{K}$ dust condensation temperature,

however, in the final gas and dust budget, we include this potential increase.

AGB stars are long period variables, whose magnitudes vary over a 100–1000 day time scale. The amplitudes of the infrared variability are smaller than those of optical variabilities: they range from 0.2 to 1.5 mag at L-band (3 μm) (Le Bertre 1992; Whitelock et al. 2006). Furthermore, mass-loss rates of AGB stars vary over time scales of 1000 years (Izumiura et al. 1996; Leão et al. 2006). The cause of long-term mass-loss rate variations are still unknown (Zijlstra et al. 2002). The variability affects our analysis for individual sourcs, but are averaged in the full, large sample.

2.2 Separation of oxygen-rich and carbon-rich AGB stars

To estimate the integrated mass-loss rates from carbon-rich AGB stars, it is essential to find a classification scheme that will separate carbon-rich from oxygen-rich stars. In particular, oxygen-rich AGB stars and red supergiants (RSGs) follow different mass-loss rate vs. colour relations from carbon-rich stars (Whitelock et al. 2006) and their dust contents will be very different.

We first compiled a list of AGB stars in the LMC observed with the Spitzer IRS by various groups (Zijlstra et al. 2006; Speck et al. 2006; Kastner et al. 2008; Leisenring et al. 2008; Sloan et al. 2008, Kemper et al. in preparation). These studies selected stars mainly from previous LMC mid-infrared surveys, *IRAS* (Schwering & Israel 1990), *MSX* (Egan et al. 2001), and surveys for long-period variables (e.g. Hughes 1989, 1990). We used the carbon- and oxygen-rich classifications quoted in these works. These are mostly based on the dust features (either silicate or SiC at 10 μm), but for stars without dust features, molecular bands are used for chemical classifications. The group of oxygen-rich stars includes both giants and super-giants, but as shown in Sect A1, two young stellar objects (YSOs) or post-AGB stars with silicate bands may contaminate the sample. We searched the photometric data in SAGE to find the counterparts to the stars observed with IRS: 122 stars have counterparts within 1 arcsec, 7 stars within 1–2 arcsec, and 5 stars have more distant counterparts. We use only identifications where the positions agree to within 2 arcsec. For the LMC this provides a total of 76 oxygen-rich and 40 carbon-rich stars from the SAGE database. We further add one oxygen-rich star (IRAS 05298−6957) from an OH maser survey in the LMC (Wood et al. 1992); the other known OH maser sources were observed with IRS. In the following figures the OH/IR star is included in 'O-AGB/RGB (IRS)'.

A catalogue of spectroscopically identified optical carbon stars in the LMC (Kontizas et al. 2001) was also searched for SAGE sources within 3 arcsec. In practice, 98 percent of the sources are found within 1 arcsec, yielding 5710 SAGE counterparts. Where there are more than two SAGE sources within 3 arcsec of the Kontizas et al. (2001) coordinates, we chose the closest one.

Cioni et al. (2001) have obtained optical spectra of 126 red stars in the LMC, and identified 11 carbon-rich and 61 oxygen-rich stars. These are described as 'C-AGB (optical)' and 'O-AGB (optical)' in the figures. We also included M-type stars (both giants and supergiants) from following works, Sanduleak & Philip (1977), Blanco et al. (1978), Westerlund et al. (1981), Wood et al. (1983, 1985), Hughes (1989), Reid et al. (1988) using coordinates taken from SIMBAD. There are 1710 objects, having 1568 counterparts in IRAC and 971 counterparts in MIPS within 1 arcsec. These stars are identified as 'O-AGB/RGB (Sim)' in the figures, although some of them could be red giant branch (RGB), rather than AGB stars.

2.2.1 Classifications involving the 8 μm band

In this section we develop a classification scheme using the $[3.6] − [8.0]$ colour to separate carbon-rich from oxygen-rich stars. Diagrams involving other colours can be found in the Appendix. Fig. 4 shows a $[3.6] − [8.0]$ vs $[8.0]$ colour magnitude diagram. The $[8.0]$-magnitudes of carbon-rich stars peak at $[3.6] − [8.0] =$2–3 mag. The SED of thick circumstellar shells peaks longward of about 7 μm.

In Fig.4 oxygen-rich stars tend to show brighter $[8.0]$-mags than carbon-rich stars at any given $[3.6] − [8.0]$, with the exception of the two oxygen-rich post-AGB/YSO candidates. Meixner et al. (2006); Blum et al. (2006) used the $[3.6] − [8.0]$ vs $[8.0]$ diagram for source classification. We also classify 'extreme-AGB stars' (Blum et al. 2006) as oxygen- or carbon-rich, based on our Spitzer IRS spectra. The boundaries which we use to separate carbon- from oxygen-rich AGB stars in Fig.4 are:

$$[8.0] > 9.0 − 1.8 \times [3.6] \ \text{ for } 0.7 < [3.6] < 2.5 \qquad (4)$$

$$[8.0] < 11.2 − 1.8 \times [3.6] \ \text{ for } 0.7 < [3.6] < 2.0 \qquad (5)$$

$$[8.0] > 4.0 − 0.2 \times [3.6] \ \text{ for } 2.0 > [3.6] \qquad (6)$$

and

$$[8.0] < 7.2 − 0.2 \times [3.6] \ \text{ for } 2.5 > [3.6]. \qquad (7)$$

This region is in general consistent with the evolutionary tracks of carbon-rich stars (Marigo et al. 2008).

In addition to low luminosity oxygen-rich stars (Sect. A1), nine IRS classified oxygen-rich stars are found in the carbon-rich region. Four of them are known to be OH/IR stars (Wood et al. 1992) and their IRS spectra show the silicate band in absorption. It is not possible to make a perfect division of the sources by this method, and inevitably some oxygen-rich sources are found in the carbon-rich region. However, this colour selection provides a method of isolating the majority of carbon-rich stars. We note that the high mass-loss rate OH/IR stars found in the carbon rich region are not expected to occur in large numbers. Furthermore, carbon-rich stars with colours similar to the OH/IR stars have lower mass-loss rates than the OH/IR stars, due to their different dust properties. Thus, the influence of blended oxygen-rich stars would be only a small perturbation on our estimate of the integrated mass-loss rate from carbon stars.
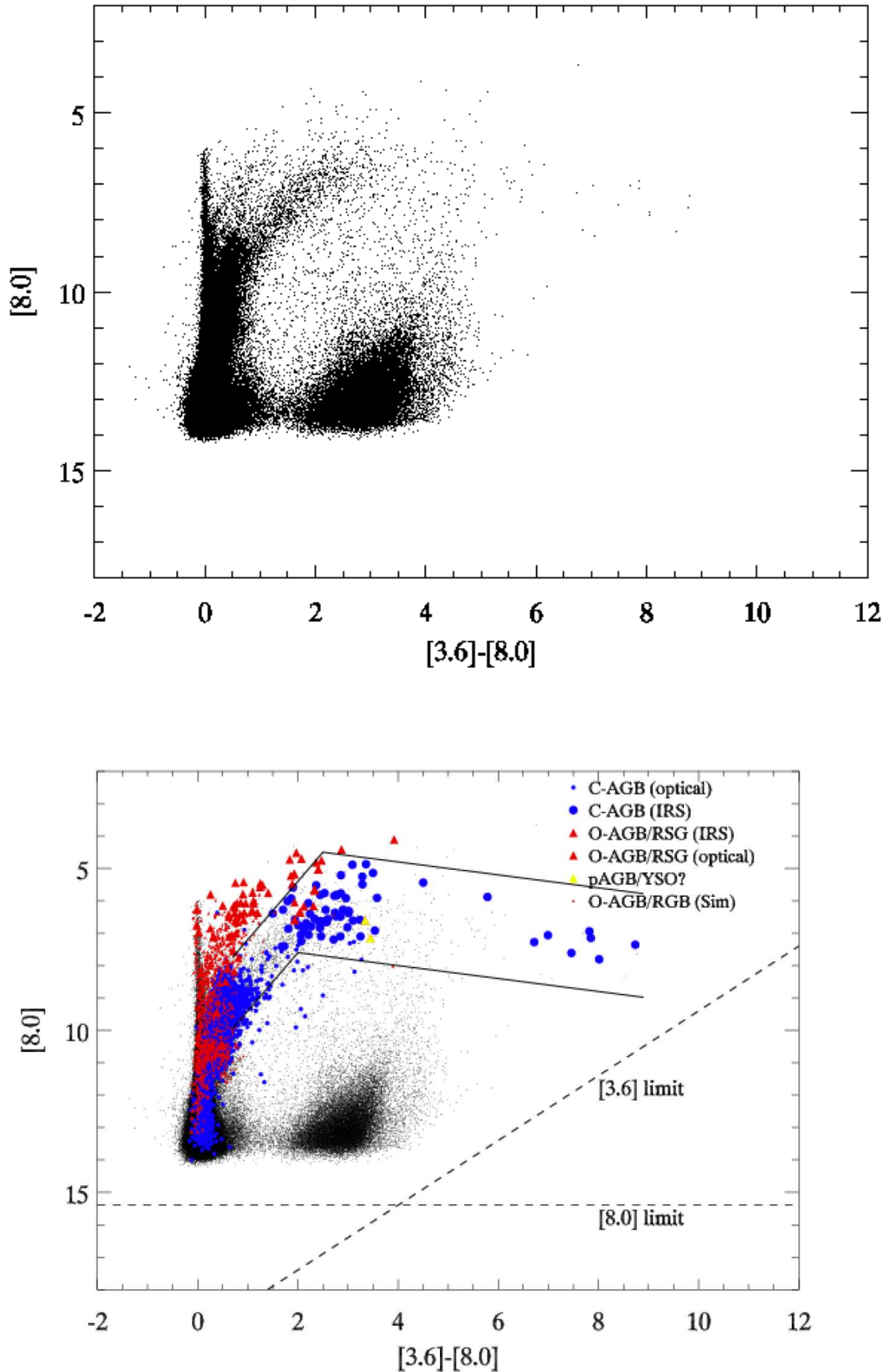
Figure 4. $[3.6] - [8.0]$ vs $[8.0]$ colour-magnitude diagram. The top panel shows the colour magnitude diagram for the complete SAGE sample. In the lower panel, spectroscopically identified oxygen-rich and carbon-rich AGB stars are plotted. The selection criteria used to identify carbon-rich AGB candidates are indicated by the solid lines. The sensitivity limits quoted by Meixner et al. (2006) for the final data product are indicated by the dashed lines. $[8.0] \sim 10.5$ likely corresponds to the tip of the RGB branch the number of carbon stars decreases at about $[3.6] - [8.0] \sim 0.7$ (at about $[8.0] \sim 9$), As seen in the top panel,

There are a large number of so called 'optical' carbon-rich stars outside the region defined by equations (4–7). However, with the available colour-colour or colour-magnitude diagrams we are unable to separate oxygen- and carbon-rich stars with thin circumstellar envelopes. Mass loss from carbon-rich stars with thin shells is discussed separately (Sect. 3.1).

At around $[3.6] − [8.0] > 4$, a small number of unresolved galaxies might intrude into the AGB star region. Blum et al. (2006) investigated the $[3.6] − [8.0]$ colours of distant galaxies. They found galaxy candidates in the red and low luminosity regime, concentrating at $[3.6] − [8.0] \sim 3$ and $[8.0] > 10$ (their fig. 7). They suggested that galaxy candidates extend up to $[8.0] \sim 7$ at $[3.6] − [8.0] \sim 3$. They did not classify point sources with $[3.6] − [8.0] \sim 3$ and $[8.0] < 10$. However, our sample based on Spitzer IRS spectra clearly shows the presence of carbon-rich stars at $[8.0] \sim 7$ at $[3.6] − [8.0] \sim 3$. We argue in Sec. 3.2 that the majority of objects with $[8.0] < 7$ and $[3.6] − [8.0] > 3$ belong to the LMC. From this we might also deduce that the most populous bright near- and mid-infrared sources in galaxies are AGB stars. This will impact the infrared colour of galaxies (Tonini et al. 2008).

There is a change in the number density of carbon stars at Ks−[8.0]∼1.4 (top panel of Fig. A3) and $[3.6] − [8.0] \sim 0.7$ (top panel of Fig. 4). This blue/red colour separation might correspond to AGB stars with and without significant mass-loss rates. For the bluer sources the opacity includes molecular bands and H^{-} continuous absorption. For the redder sources, dust emission contributes to the mid-infrared excess. Indeed, IRAS observations show a $[12] − [25]$ gap between $−1.2$ and $−1.4$ (van der Veen & Habing 1988) and stars redder than $−1.4$ are those with dust-driven mass loss[1]. The gap can be understood as the separation of huge numbers of stars with very little mass loss from those with circumstellar envelopes. Once dust grains have condensed, mass-loss rates increase drastically (van der Veen & Habing 1988), as do colours. The $Ks − [8.0]$ and $[3.6] − [8.0]$ do not show the obvious gap seen in $[12] − [25]$, as the influence of dust on the [8.0]-band is not strong, but it is likely that the decrease in stellar density is related to the increase in mass-loss rate.

Possible sources of contamination for our carbon-rich AGB sample include H II regions. Kastner et al. (2008) have classified bright objects in the MSX A-band, which covers $8 \, \mu m$, and they found four H II regions in the range $4.0 < A < 6.5$ and $6 < K − A < 9$. Although the MSX A- and Spitzer [8.0]-bands are not identical, the wavelength coverage is similar, suggesting H II regions could be a contaminant. A search for cross-identifications of SIMBAD sources within three arcsec revealed one H II region, five Be stars or emission-line objects, two YSOs, three molecular clouds, one sym-

biotic star (essentially an AGB star with a compact companion), two planetary nebulae (PNe), and one WR star. Whitney et al. (2008) showed that luminous YSOs cross the AGB sequence, but we expect the high mass YSO population to be significantly smaller than that of AGB stars. The initial masses of carbon-rich AGB stars are about 1.5–$5.0 \, M_{\odot}$ (Vassiliadis & Wood 1993), while YSOs, which can reach $[8.0] < 8$, have masses higher than $10 \, M_{\odot}$. Using the IMF from Kroupa (2001), with an exponent of $\alpha = 1.3$, and assuming a constant star formation rate, stars with 1.5–$5.0 \, M_{\odot}$ have a birth rate ten times higher than stars with masses greater than $10 \, M_{\odot}$, although the SFR might vary (Feast 1995). The lifetime of such high mass YSO is also much shorter than that of the AGB phase. Similarly WR stars have high initial-masses and their numbers should be low. PNe (and most symbiotic stars) are usually located outside of our carbon-rich region, and are more concentrated at lower [8.0]-band luminosities (Hora et al. 2008, who used the most complete PN catalogue from Reid & Parker (2006)). We expect that because their lifetimes are short, the PN contamination is low.

The sensitivity limits of the surveys are shown on the colour-magnitude diagrams. These sensitivities ($5 \, \sigma$ detection limits) are those for the final product taken from Skrutskie et al. (2006) and Meixner et al. (2006); note that the actual detection limits of the catalogues used could be lower than those illustrated here. The Spitzer SAGE project includes observations of the LMC at two epochs, but the catalogue used (2007 Winter version) contains only data from the first of epoch (Meixner et al. 2006). In Fig. A1, the sensitivity ($5 \, \sigma$ detection) limits of the 2MASS survey (Skrutskie et al. 2006) are plotted on the diagram. The 2MASS sensitivity is not high enough to detect the reddest part of the carbon-rich sequence.

3 RESULTS

3.1 Mass-loss rates for all carbon-rich AGB candidates

The mass-loss rates for carbon-rich stars are estimated using the colour vs mass-loss-rate relations derived in Sect. 2.1. The stars with high mass-loss rates are listed in Table 1. We assume that statistically these relations will give an integrated mass-loss rate for all carbon-rich mass-losing AGB candidates. Specifically, we use $[3.6] − [8.0]$, supplemented by $Ks − [8.0]$ for low mass-loss rate stars, to estimate the rates.

There are 1779 carbon-rich AGB candidates with $[3.6] − [8.0] > 0.7 \, \mathrm{mag}$. The integrated mass-loss rate from all 1779 stars, derived from this colour, is $7.4 \times 10^{-3} \, M_{\odot} \, \mathrm{yr}^{-1}$. The highest individual mass-loss rate is $9.3 \times 10^{-5} \, M_{\odot} \, \mathrm{yr}^{-1}$. The upper limit may be set by the detection limit in the [3.8]-band (Figs. 4 and A7). The distribution of stars amongst the mass-loss rate ranges is summarized in Table 2.

For stars with low mass-loss rates, the fits to colour vs mass-loss rate using the two different colours, $Ks − [8.0]$ and $[3.6] − [8.0] > 0.7$, give slightly different results; this is because towards blue colours, the

---

[1] In the van der Veen et al. study the IRAS bands are not normalized with zero-magnitudes, but $[12] − [25]$ is defined by $2.5 \log(F_{25}/F_{12})$, where F_{12} and F_{25} are the IRAS fluxes in Jy in the 12 and 25 μm bands.

Table 1. LMC carbon-rich AGB candidates with high mass-loss rate ($> 1 \times 10^{-5}\, M_\odot\, \mathrm{yr}^{-1}$). The full table is available in on-line.

SAGE name	J (mag)	H (mag)	K (mag)	[3.6] (mag)	[4.5] (mag)	[5.8] (mag)	[8.0] (mag)	[24] (mag)	$\dot{M}_{g2}$ ($M_\odot\, \mathrm{yr}^{-1}$)
J045013.14−693356.7	15.681	15.784	14.348	12.182	10.938	9.537	7.764	3.274	2.7×10^{-5}
J045358.59−691106.3	—	15.774	14.194	11.392	10.603	8.865	7.273	1.008	2.3×10^{-5}
J045842.03−680715.3	—	—	—	10.323	8.539	7.078	5.765	3.695	2.9×10^{-5}
J045935.79−682444.7	15.205	14.491	13.567	10.398	9.328	8.307	7.278	6.319	1.1×10^{-5}
J043257.38−692633.0	—	—	14.323	10.124	8.688	7.505	6.453	4.535	1.7×10^{-5}
J045613.48−693230.9	—	—	—	10.637	8.915	7.557	6.363	4.143	2.5×10^{-5}
J045845.98−682037.7	—	—	—	10.741	8.877	7.403	6.076	3.662	3.1×10^{-5}
J044854.41−690948.1	—	—	13.880	11.530	10.646	9.245	7.594	1.656	2.1×10^{-5}
J044650.41−675124.2	—	—	13.956	10.428	9.227	8.274	7.373	5.796	1.0×10^{-5}
J045433.84−692036.1	14.357	13.594	12.414	9.947	8.958	7.982	6.606	3.904	1.3×10^{-5}

Table 4. Overall properties of the LMC

	All surveyed area	Bar	Bar cent	Disk
Total number of carbon-rich AGB candidates	1779	1194	517	585
Integrated mass-loss rate‡ ($\times 10^{-4}\, M_\odot\, \mathrm{yr}^{-1}$)	86	59	23	27
Area (deg^2)	50.4	18.7	5.7	31.7
Mass-loss rate per unit area ($\times 10^{-4}\, M_\odot\, \mathrm{yr}^{-1}\, \mathrm{deg}^{-2}$)	1.7	3.2	4.1	0.8
Same as above but in different units ($\times 10^{-4}\, M_\odot\, \mathrm{yr}^{-1}\, \mathrm{kpc}^{-2}$)	2.2	4.0	5.1	1.1

The mass-loss rates from carbon-rich AGB stars could be underestimated by a factor of up to 2.4, due to the unknown dust condensation temperature (Sect 2.1).‡ gas mass-loss rates are estimated using $Ks - [8.0]$ and $[3.6] - [8.0]$.

Table 2. Number distribution of mass-losing carbon-rich candidates in the LMC. Two different colours ($Ks - [8.0]$ and $[3.6] - [8.0]$) were used to estimate the mass-loss rates of individual stars. In the last column, one or other of these colours were used, i.e., if $[3.6] - [8.0] < 2.2$, $Ks - [8.0]$ vs mass-loss rate relation was adopted, otherwise the $[3.6] - [8.0]$ vs mass-loss rate relation was used. The total gas mass-loss rate is obtained by integrating the mass-loss rates of individual stars.

$\dot{M}_g$ range	$\dot{M}_{g1}$		$\dot{M}_{g2}$	
	N	Total $\dot{M}_g$	N	Total $\dot{M}_g$
($M_\odot\, \mathrm{yr}^{-1}$)		($10^{-4}\, M_\odot\, \mathrm{yr}^{-1}$)		($10^{-4}\, M_\odot\, \mathrm{yr}^{-1}$)
$\dot{M}_g < 1 \times 10^{-6}$	996	3‡	588	4†
$1 \times 10^{-6} < \dot{M}_g < 3 \times 10^{-6}$	298	5	522	10
$3 \times 10^{-6} < \dot{M}_g < 6 \times 10^{-6}$	188	8	352	14
$6 \times 10^{-6} < \dot{M}_g < 1 \times 10^{-5}$	109	9	122	9
$1 \times 10^{-5} < \dot{M}_g < 3 \times 10^{-5}$	140	24	140	24
$3 \times 10^{-5} < \dot{M}_g < 6 \times 10^{-5}$	39	15	39	15
$6 \times 10^{-5} < \dot{M}_g < 1 \times 10^{-4}$	13	10	13	10
Total	1779	74§	1779	86§

$\dot{M}_g$: gas mass-loss rates, assuming a gas-to-dust mass ratio of 200
N: number of stars
$\dot{M}_{g1}$: $\dot{M}_g$ estimated from $[3.6] - [8.0]$ only
$\dot{M}_{g2}$: $\dot{M}_g$ estimated from $Ks - [8.0]$ and $[3.6] - [8.0]$
‡ The minimum mass-loss rate is $4 \times 10^{-8}\, M_\odot\, \mathrm{yr}^{-1}$, limited by $[3.6] - [8.0] > 0.7\,\mathrm{mag}$
† The minimum mass-loss rate is $4 \times 10^{-8}\, M_\odot\, \mathrm{yr}^{-1}$, limited by $Ks - [8.0] > 1.4\,\mathrm{mag}$ (as well as $[3.6] - [8.0] > 0.7\,\mathrm{mag}$).
§ Due to rounding, adding $\dot{M}_g$ in seven ranges does not give the identical number as the total $\dot{M}_g$.

Table 3. Number distribution of LMC carbon-rich candidates as a function of mass-loss rates based on $[3.6] - [8.0]$ and $Ks - [8.0]$ colours in the entire SAGE survey area, the bar region, the bar centre, and the remainder of the surveyed area except of the bar region (quoted as 'disk')

$\dot{M}_{g2}$ range	Number fraction of stars			
	All	Bar	Bar cent.	Disk
($M_\odot\, \mathrm{yr}^{-1}$)				
$4 \times 10^{-8} < \dot{M}_g < 1 \times 10^{-6}$	33 %	32 %	35 %	35 %
$1 \times 10^{-6} < \dot{M}_g < 3 \times 10^{-6}$	31 %	31 %	32 %	31 %
$3 \times 10^{-6} < \dot{M}_g < 6 \times 10^{-6}$	18 %	19 %	19 %	17 %
$6 \times 10^{-6} < \dot{M}_g < 1 \times 10^{-5}$	7 %	7 %	6 %	7 %
$1 \times 10^{-5} < \dot{M}_g < 3 \times 10^{-5}$	8 %	9 %	7 %	7 %
$3 \times 10^{-5} < \dot{M}_g < 6 \times 10^{-5}$	2 %	2 %	2 %	2 %
$6 \times 10^{-5} < \dot{M}_g < 1 \times 10^{-4}$	0.7 %	0.8 %	0.8 %	0.7 %
Total N	1779	1194	517	585

$\dot{M}_{g2}$: gas mass-loss rates estimated using $Ks - [8.0]$ and $[3.6] - [8.0]$
N: number of stars
Percentages over the seven ranges do not sum to 100 % due to rounding.

extrapolated relations are poorly defined. $Ks - [8.0]$ is probably better for these low mass-loss rate stars. We combine the two estimates of the mass-loss rate as follows: We adopt the estimate from $[3.6] - [8.0]$ for stars with $[3.6] - [8.0] > 2.2$, otherwise we take the rates from $Ks - [8.0]$. If a star does not have a Ks-band magnitude, we use the rates from $[3.6] - [8.0]$. Above $[3.6] - [8.0] > 2.2$ ($\sim 3 \times 10^{-6}\, M_\odot\, \mathrm{yr}^{-1}$) up to Ks detection limit, the mass-loss rates from the two colours

are essentially identical. This procedure gives an integrated mass-loss rate of $8.6 \times 10^{-3}\,M_\odot\,\mathrm{yr}^{-1}$, as summarized in the last column of Table 2. This combined method only makes a 10 % difference in the integrated mass-loss rate from that using the $[3.6] - [8.0]$ relation alone, as the low mass-loss rate stars contribute little to the integrated value.

Independent work with a totally different approach by Srinivasan et al. (2008) obtained a similar integrated mass-loss rate for AGB stars ($2.5 \times 10^{-3}\,M_\odot\,\mathrm{yr}^{-1}$). Our estimate is higher, because we included stars with extremely high mass-loss rates, which had not been categorized before (Blum et al. 2006), but were found to be carbon-rich AGB stars recently (Gruendl et al. 2008).

Because of the sensitivity limit in the Ks-band (Fig. A3), and possibly in the [3.6]-band (Fig. A7), it is possible that not all AGB stars with extremely high mass-loss rates will have been detected. Therefore the integrated mass-loss rate derived above might be considered a lower limit.

Table 2 shows the number distribution per mass-loss rate range among carbon-rich AGB candidates, combining the two infrared colour estimates. Stars with relatively high mass-loss rates ($> 6.0 \times 10^{-6}\,M_\odot\,\mathrm{yr}^{-1}$) are responsible for most of the integrated mass loss. A similar result was found for Galactic AGB stars (Knapp & Morris 1985; Jura & Kleinmann 1989; Le Bertre et al. 2001; Ojha et al. 2007).

There are 1779 carbon-rich AGB candidates in the LMC (Sec.2.2) selected by $[3.6] - [8.0] > 0.7$. The number of AGB stars with $[3.6] - [8.0] < 0.7$ is almost 10 times greater than that with $[3.6] - [8.0] > 0.7$. In the region of $10.5 < [8.0] < 8$ and $[3.6] - [8.0] < 0.7$, there are 13460 stars, where we assume that $[8.0] \sim 10.5$ corresponds to the tip of the RGB branch *(as the number of stars decreases at $[8.0] < 10.5$; Fig. 4)*, and where both oxygen-rich and carbon-rich stars are mixed together. Furthermore, there are carbon-rich AGB stars below the tip of the RGB ($[8.0] < 10.5$) (Lagadec et al. 2007), which are uncounted due to the confusion with RGB stars. These will be a mixture of extrinsic carbon-stars, which have become carbon-rich due to mass-transfer from an evolved companion, or AGB stars in the brief phase of low luminosity which follows a helium shell flash. Extrinsic carbon stars should not be included in our census. The numbers of the others could be significant, but their mass-loss rates are low. The boundary at $[3.6] - [8.0] \sim 0.5$ may be separating stars with dust-driven winds from those with pulsation/opacity driven mass loss. If we assume a plausible mass-loss rate of $1 \times 10^{-8}\,M_\odot\,\mathrm{yr}^{-1}$ on average, similar to red-giant branch stars (10^{-9}–$10^{-8}\,M_\odot\,\mathrm{yr}^{-1}$), the integrated mass-loss rate from these stars would be $\sim 1 \times 10^{-4}\,M_\odot\,\mathrm{yr}^{-1}$, a minor contribution to the integrated mass-loss rate. These are very rough estimates, and we do not include them into the final number.

3.2 Spatial distribution of carbon-rich stars

Fig. 5 and Table 3 show the distribution of carbon-rich AGB stars with intermediate and high mass-loss rates within various parts of the LMC. The areas are specified
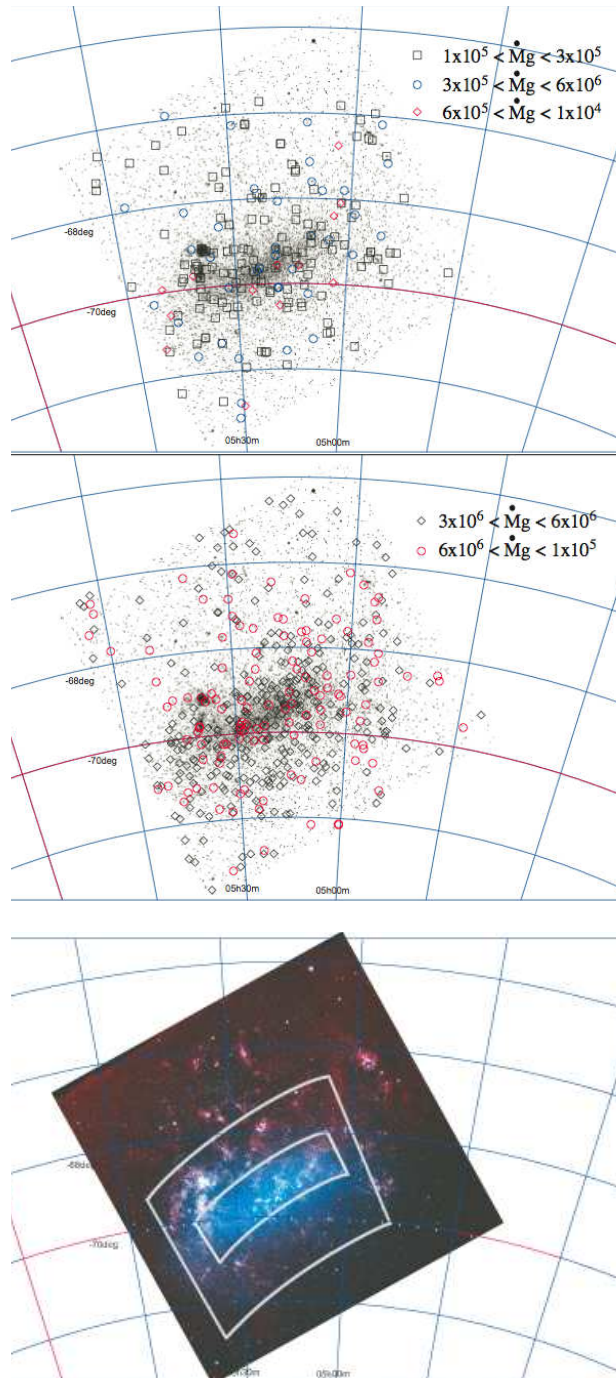

Figure 5. The spatial distribution of mass-losing carbon-rich AGB candidates in the LMC is plotted over the SAGE 3.6 μm image (top and middle). Candidates are classified into groups according to mass-loss rate as given on the figure. Carbon-rich AGB candidates are concentrated in the LMC bar. In the bottom panel, large and small rectangles show the areas defined for the 'bar' and the 'bar centre', as used in our analysis. (on-line version, the bottom panel is the SAGE 3-color composition image (Meixner et al. 2006): 3.6 μm image for blue, 4.5 μm image for green and 5.8 μm for red. The LMC bar region is found in blue color, as stellar components are dominant.)

in the lower panel of Fig. 5. The majority of the stars are located towards the LMC bar.

One-third of the mass-losing carbon-rich AGB candidates are concentrated in the bar centre. This is consistent with the findings from near-infrared surveys, which show a high concentration of carbon-rich stars in the bar (Blanco et al. 1978; Cioni et al. 2006a).

There are at least two regions containing clusters, NGC 2154 (RA=05h57m38s, Dec=−67º15.7′, J2000), where about 44 carbon-rich stars have been reported (Blanco et al. 1978), and NGC 1978 (RA=05h27m17s, Dec=−70º44.1′, J2000), where about 24 carbon stars have been found by Westerlund et al. (1991), and which contains a carbon-rich AGB Mira variable (Tanabé et al. 1997).

4 DISCUSSION

4.1 Mass-loss rates from AGB stars per unit area

Using the result listed in Table 4 for the LMC the integrated mass-loss rate is $2.2 \times 10^{-4}\,M_\odot\,\mathrm{yr}^{-1}\,\mathrm{kpc}^{-2}$ for carbon-rich AGB candidates only. There is a spatial variation in the range 1.1–$5.1 \times 10^{-4}\,M_\odot\,\mathrm{yr}^{-1}\,\mathrm{kpc}^{-2}$. This value is comparable to that found in the solar neighbourhood, where Jura & Kleinmann (1989) investigated AGB stars within $\sim 1\,\mathrm{kpc}$ from the Sun and obtained an integrated mass-loss rate from AGB stars of 3–$6 \times 10^{-4}\,M_\odot\,\mathrm{yr}^{-1}\,\mathrm{kpc}^{-2}$. Their study was limited to stars with $\dot{M}_g > 2 \times 10^{-6}\,M_\odot\,\mathrm{yr}^{-1}$, but lower mass-loss rate stars would not contribute to the value significantly. Half of the mass was from oxygen-rich and the other half from carbon-rich AGB stars. Thronson et al. (1987), Tielens (1990) and Groenewegen et al. (1992) obtained similar numbers for the gas injection rate from carbon-rich AGB stars in the Galaxy. Assuming that the gas-to-dust ratios are comparable in these two galaxies, the gas mass per unit area injected from carbon-rich stars in the Galactic plane and the LMC bar centre are similar.

4.2 Other gas and dust sources in the LMC

For comparison with the result discussed above, we estimate the gas and dust mass expelled from other sources in the LMC and summarize the findings in Table 5.

4.2.1 Gas and dust injection from SNe

We estimate the gas output from SNe based on the theoretical model of Kodama & Arimoto (1997). We use the revised IMF from Kroupa (2001) (lower mass limit: $M_{\mathrm{lo}} = 0.1\,M_\odot$ and upper mass limit: $M_{\mathrm{up}} = 60\,M_\odot$), and assume a constant star formation rate (SFR) over the past few Myr which is the same as the current value. Under these conditions, the ratio of the SFR to the gas expulsion rate (GER) by type II SNe is 0.32. Smecker-Hane et al. (2002) measured the SFR using red giants, which date from as recently as 200 Myr ago; we adopt this as the current value. They gave SFRs of $0.01\,M_\odot\,\mathrm{yr}^{-1}\,\mathrm{deg}^{-2}$ and $0.004\,M_\odot\,\mathrm{yr}^{-1}\,\mathrm{deg}^{-2}$ in the

bar and disk regions, respectively. These numbers result in SN gas inputs to the ISM of $3 \times 10^{-3}\,M_\odot\,\mathrm{yr}^{-1}\,\mathrm{deg}^{-2}$ in the bar and $1 \times 10^{-4}\,M_\odot\,\mathrm{yr}^{-1}\,\mathrm{deg}^{-2}$ in the disk. This implies that, in the bar, the gas injection rate from SNe is higher than that from AGB stars, but AGB stars are more important in the disk, if oxygen-rich stars are counted. The fact that supernova remnants (SNRs) are concentrated around the bar region and 30 Dor (Williams et al. 1999) supports this conclusion.

In the following we use the SN rate estimated from the number of SNRs and the dust mass observed from SNe and SNRs. Mathewson et al. (1983) list 25 SNRs in the LMC. They estimated the frequency of type II SNe as one per 275 yrs, and for type I SNe as approximately one per 550 yrs. More recently, Williams et al. (1999) added a further 6 SNRs. Although their SN type is unknown, they are more likely to be Type II, because galaxy chemical evolution models suggest that Type Ia and Type II occur with a ratio of about 0.3 in the LMC (Tsujimoto et al. 1995). Filipović et al. (1998) estimated an LMC SNR rate of one in every 100 yrs. The Type II SN rate (for both type I and II) of Mathewson et al. (1983) remains valid, but the time interval could be shorter by up to 145 yrs.

The dust output from SNe remains uncertain. The famous type II SN in the LMC, SN 1987A, emitted a significant infrared excess from dust grains (Moseley et al. 1989; Whitelock et al. 1989). The highest estimate of the dust mass from SN 1987A is $1.3 \times 10^{-3}\,M_\odot$ (Ercolano et al. 2007). Based on this value, type II SNe could produce up to $5 \times 10^{-6}\,M_\odot\,\mathrm{yr}^{-1}$ of new dust. In the SMC dust mass of $8 \times 10^{-4}\,M_\odot$ is found in a SNR (Stanimirović et al. 2005). Even higher dust masses have been reported from other type II SNe in other galaxies: $0.02\,M_\odot$ in SN 2003gd in NGC 628 (Sugerman et al. 2006) and 0.02–$0.05\,M_\odot$ in Cas A (Rho et al. 2008). A lower dust mass has been suggested for SN 2003gd ($4 \times 10^{-5}\,M_\odot$; Meikle et al. 2007). Sakon et al. (2008) estimated a dust mass of 2.2–$3.4 \times 10^{-3}\,M_\odot$ produced from SN 2006jc. These estimates give a range of $(0.1$–$130) \times 10^{-4}\,M_\odot\,\mathrm{yr}^{-1}$ for the dust mass from observations of SNe and SNRs. The dust mass produced by SNe remains very uncertain for the following reasons: extinction measurements give a column density rather than a mass; the mid-infrared photometric measurements are mainly sensitive to warm dust at the early phase, and may need to be corrected for flash-heated interstellar dust; sub-mm measurements probe cold dust, but can be confused with interstellar dust clouds. The clumping is also uncertain and affects the mass determination. Finally, the primary dust production by SNe may be significantly counteracted by subsequent dust destruction when the ejecta hits the ISM (Jones et al. 1994; Dwek 2008), which is not considered here. The dust production given here for SNe is tentative, and could change by an order of magnitude or more.

We adopt a lower limit for the progenitor mass of Type II SNe of $8\,M_\odot$ (Smartt et al. 2008), and the IMF from Kroupa (2001), with a GER/SFR through SNe of 0.32. Then, with a SN rate of one per 145–275 yrs, the gas ejection rate from Type II SNe is 0.02–

Table 5. Gas and dust injected into the ISM of the LMC

Sources	Gas mass $(10^{-3}\,M_\odot\,\mathrm{yr}^{-1})$	Dust mass $(10^{-6}\,M_\odot\,\mathrm{yr}^{-1})$	Chemical type
AGB stars			
Carbon-rich	8.6 (up to 20.6§)	43 (up to 100)	C-rich
Oxygen-rich	>>2†	>>0.4†	O-rich
Type II SNe	20–40	0.1–130‡	both O- and C-rich
WR stars	0.6		(C-rich?)
Red supergiants	>1	>2	O-rich

§ Considering the unknown dust condensation temperature, mass-loss rate can be underestimated by a factor of up to 2.4 (Sect 2.1)
† The number listed is the lower limit obtained from the observations. Expected gas and dust mass-loss rate are
$8.6 \times 10^{-3}\,M_\odot\,\mathrm{yr}^{-1}$ and $1.2 \times 10^{-5}\,M_\odot\,\mathrm{yr}^{-1}$, respectively.
‡ Dust production (or possibly destruction) in and around SNe remains uncertain.

$0.04\,M_\odot\,\mathrm{yr}^{-1}$. This is higher than the integrated gas mass-loss rate from carbon-rich AGB candidates. This number critically depends on the progenitor mass range of SNe (see discussion in Smartt et al. 2008). Type Ib/c SNe may also contribute to core-collapse SNe and are not counted here as their origin remains uncertain.

4.2.2 WR stars and LBVs

Breysacher et al. (1999) published a catalogue of Population-I Wolf-Rayet (WR) stars in the LMC. Among 134 stars, gas mass-loss rates are given for 40, most of which were measured by Crowther & Smith (1997). Simply integrating these 40 stars gives $2 \times 10^{-3}\,M_\odot\,\mathrm{yr}^{-1}$. If the remaining 74 stars have similar mass-loss rates on average, we expect about $6 \times 10^{-3}\,M_\odot\,\mathrm{yr}^{-1}$ from Population-I WR stars in total. There are over a hundred suspected WR stars in the LMC, so the gas mass-loss rate from WR stars may be underestimated by a factor of up to a few. Late-type WR stars (WC7–WC9) produce dust, but no such stars have been found in the LMC (Smith et al. 1988; Moffat 1991).

Luminous Blue Variables (LBVs) could also potentially contribute to the gas and dust injected into the ISM. Zickgraf (2006) listed 15 B[e] supergiants in the LMC and Van Genderen (2001) listed 21 S Dor variables. However, the mass-loss rates of these stars are still unknown. Well studied objects of this type in the Galaxy include η Car and AG Car. Hillier et al. (2001) suggested a gas mass-loss rate of $1 \times 10^{-3}\,M_\odot\,\mathrm{yr}^{-1}$ for η Car using a formula from Wright & Barlow (1975); near-infrared interferometric observations suggested $1.6 \times 10^{-3}\,M_\odot\,\mathrm{yr}^{-1}$ (van Boekel et al. 2003) for η Car. Voors et al. (2000) estimated a dust mass-loss rate of $3 \times 10^{-5}\,M_\odot\,\mathrm{yr}^{-1}$ for AG Car from mid- and far-infrared observations. However, it is clear that not all LBVs have dust mass-loss rates as high as η Car and fewer than half of the objects have noticeable excesses (Van Genderen 2001).

Winds from OB-type stars could contribute to the gas enrichment process in the ISM. Bastian et al. (2009) estimated about 2000 OB stars to be present within the inner 3 degree radius of the LMC. This area is similar in size to the SAGE survey coverage. If OB stars

have mass-loss rates up to 1×10^{-7}–$1 \times 10^{-6}\,M_\odot\,\mathrm{yr}^{-1}$ (Evans et al. 2004), the total gas lost from OB stars could be 2×10^{-4}–$2 \times 10^{-3}\,M_\odot\,\mathrm{yr}^{-1}$.

4.2.3 Red supergiants

High mass stars (more than $8\,M_\odot$) can produce dust grains during their red supergiant phase (e.g. Verhoelst et al. 2009). One of the most luminous red supergiants (RSGs) in the LMC is WOH G64 and its circumstellar dust mass could be as high as $2 \times 10^{-2}\,M_\odot$ (Ohnaka et al. 2008). This exceeds the total dust production from SN 1987A. van Loon et al. (2005) listed 14 oxygen-rich red supergiants, which exceed the classical upper limit of AGB luminosity, i.e. $\log L(L_\odot) = 4.74$ (c.f. Wood et al. 1983). The combined gas mass-loss rates of these 14 stars is $1 \times 10^{-3}\,M_\odot\,\mathrm{yr}^{-1}$. A gas-to-dust ratio of 500 was assumed in their work (van Loon et al. 1999). The dust mass-loss rate from RSGs amounts to $2 \times 10^{-6}\,M_\odot\,\mathrm{yr}^{-1}$.

Previous studies mainly depend on the IRAS survey. After an investigation of RSGs using SAGE data (Kemper et al. in preparation), the number of known RSGs may increase. The integrated mass-loss rate for the RSGs quoted here is therefore likely to be a lower limit.

4.2.4 Oxygen-rich AGB stars

The total number of oxygen-rich AGB stars with circumstellar envelopes is unknown. Thus, their total mass-loss rate remains essentially unknown. van Loon et al. (2005) discuss 7 oxygen-rich AGB stars and from these we obtain an integrated mass-loss rate of $2 \times 10^{-4}\,M_\odot\,\mathrm{yr}^{-1}$ in gas and $0.4 \times 10^{-6}\,M_\odot\,\mathrm{yr}^{-1}$ in dust, assuming a gas-to-dust ratio of 500 as in the original work (van Loon et al. 1999). The gas-to-dust ratio of oxygen-rich AGB stars is unknown, but as silicon atoms are not synthesised in AGB stars, the silicate dust amount can be assumed to correlate with the original silicate abundance of the star. It is expected that the gas-to-dust ratios of oxygen-rich AGB stars are lower in the LMC than in our Galaxy, as a similar trend was found in the ISM. These provide a lower limit to the integrated mass-loss rates; further estimates can be made

after the IRS followup of SAGE is completed (Kemper in preparation).

We expect that the upper limits of gas and dust input from oxygen-rich stars are comparable to the values from carbon-rich stars, simply from the relative numbers of objects. It is known that the number ratio of oxygen-rich stars and carbon-rich stars depends on the metallicities (Feast 1989, 2006; Groenewegen 2007, e.g.) In the LMC, among AGB stars with low mass-loss rates there are as many oxygen-rich as carbon-rich stars (Blanco et al. 1978). However, among PNe, the next evolutionary phase, there are only two oxygen-rich dusty sources found out of 23 PNe (Stanghellini et al. 2007; Bernard-Salas et al. 2008). Thus, the integrated mass-loss rate from oxygen-rich AGB stars is expected to be similar to or less than that from carbon-rich stars. Further, stellar evolutionary models predict that oxygen-rich stars evolve from both low-mass (1.0–$1.5\,M_\odot$ on the main sequence) and intermediate mass (5.0–$8.0\,M_\odot$) progenitors, while carbon stars originate from 1.5–$5.0\,M_\odot$ at the LMC metallicity (Karakas & Lattanzio 2007). Many intermediate-mass oxygen-rich stars will have experienced hot bottom burning (Boothroyd et al. 1993), turning carbon atoms into oxygen atoms. Kroupa (2001)'s IMF gives an oxygen- and carbon-rich ratio of 1:1 in number, but 1:1.4 in mass. Hence our conclusion is that the integrated mass-loss rate from oxygen-rich AGB stars is expected to be similar to or less (approximately $6 \times 10^{-3}\,M_\odot$) than that from carbon-rich AGB stars.

Lagadec & Zijlstra (2008a) argue that at low metallicity, oxygen-rich dust drives a superwind only when the stellar luminosity exceeds a crictical value, of the order of $10^4\,L_\odot$ for the case of the LMC. This would predict that the mass loss is more dominated by carbon stars than their number ratio would suggest.

Among AGB stars, S-type stars represent stars with a C/O ratio close to unity. This type of star are considered to trace a transiting phase from oxygen-rich stars to carbon-rich stars. In the LMC, there is no complete sensus of S-type stars; a few stars are listed in Cioni et al. (2001). In our Galaxy, the fraction of S-type stars is assumed to be 1 % of total AGB population. Thus, we assume gas and dust lost from S-type stars is relatively minor. Except for a few SC-type stars (Aoki et al. 1998), which have a carbon-rich atmosphere, S-type stars tend to produce some silicate dust (Little-Marenin & Little 1988; Chen & Kwok 1993).

4.3   Gas and dust sources in the LMC

Table 5 summarizes the estimated gas and dust production from various sources. AGB stars are one of the main sources of the dust enrichment for the ISM of the LMC, and carbon-rich AGB stars are a major factor. The dust contribution from SNe is very uncertain. There could also be minor inputs from novae and R CrB stars. Dust evolution models show that within our Galaxy carbon dust originates mainly from carbon-rich AGB stars (Dwek 1998; Zhukovska et al. 2008). Our work shows that dust production in the LMC follows a similar trend.

If a gas-to-dust ratio of 200 is valid for carbon-rich

AGB stars, and our estimates for mass loss from SNe are correct, AGB stars are as important a gas contributor as are SNe. SN activity is concentrated towards the 30 Dor and LMC bar region. In the LMC disk, AGB stars could be the more important source of gas and dust. Other sources appear to present minor contributions to the ISM enrichment.

This result is in marked contrast to our Galaxy where AGB stars are thought to be the main source, even for gas (Tielens et al. 2005). The contribution from SNe is an order of magnitude smaller than that of AGB stars. The observational difference can be related to the recent increase in the star formation rate (SFR; Smecker-Hane et al. 2002) in the LMC bar region, which has been suggested to be due to the tidal interaction with the SMC (Bekki & Chiba 2005). Indeed, assuming a constant SFR and using the IMF, we find that the gas injection rate from AGB stars should be a factor of twice larger than that from SNe and their precursors. Thus an increase of the SFR appears to be required in the LMC.

4.4   Populations and spatial distributions

Table 3 shows, as a function of mass-loss rate, the number distributions for carbon-rich AGB candidates in the bar, the bar centre, outside of the bar, and the entire area surveyed. We have defined the bar centre and bar regions as shown in Fig. 5. The fraction of stars with different mass-loss rates shows little dependence on their location within the LMC. This suggests that most of these stars belong to a similar population. Contamination by non-LMC objects, i.e., distant galaxies, should be minimal; the number density of distant galaxies is almost uniform and thus the number counted should be proportional to the area examined.

Reid & Parker (2006) surveyed PNe in the LMC using narrow-band optical filters. They found fewer PNe in the north part of the bar (between 5h45m, $-68°30'$ and 5h15m, $-67°15'$) than in the surrounding area, and concluded that interstellar extinction towards this region is responsible for the lower number density. However, a similar trend is found for the AGB-star distribution, despite the fact that extinction in the near- and mid-infrared will be negligible. Generally, in comparison to the age of galaxies, AGB stars and PNe belong to similar stellar populations. Thus, this absence of PNe and AGB stars in the north part of the bar appears to be intrinsic to the LMC.

A distinct component of the population is also found among young red supergiants; fig. 2 in Cioni et al. (2000a) shows a secondary peak at about Dec $> -67°$ which presumably corresponds to stars younger than 0.5 Gyrs. Similarly, high mass-loss rate AGB stars (rates between $6 \times 10^{-6}\,M_\odot\,\mathrm{yr}^{-1}$ and $3 \times 10^{-4}\,M_\odot\,\mathrm{yr}^{-1}$) are populous in that region, although they are absent in the northern part of the bar. In this region, stars with low and intermediate mass-loss rates (from $3 \times 10^{-6}\,M_\odot\,\mathrm{yr}^{-1}$ to $6 \times 10^{-6}\,M_\odot\,\mathrm{yr}^{-1}$) are under-populated. This may suggest that the location of active star forming regions has not changed significantly over the past 0.5–1 Gyrs.

Oxygen-rich AGB stars originate both from relatively low mass (1.0–$1.5\,M_\odot$) and relatively high mass (5.0–$8.0\,M_\odot$) stars, at the LMC metallicity (Karakas & Lattanzio 2007). The distribution of oxygen-rich and carbon-rich stars might differ from each other, as the majority of the oxygen-rich stars (which belong to a lower mass group), belong to an older population. Indeed, Blanco et al. (1978) and Cioni et al. (2006a) showed that oxygen-rich stars spread further out into the disk region than do carbon-rich stars.

Based on optical imaging and a population synthesis model, Smecker-Hane et al. (2002) suggested that in the bar region 35 percent of the stars are younger than 3 Gyr, and 71 percent are younger than 7.5 Gyr. In contrast, the disk has an older population, as the corresponding numbers are 19 percent and 41 percent. The initial masses of carbon-rich stars are 1.5–$5.0\,M_\odot$ (Vassiliadis & Wood 1993; Stancliffe et al. 2005). These stars reach the thermal pulsating AGB phase in under 3 Gyr. Our observations show that the carbon-rich AGB candidates are concentrated in the bar, which is consistent with a population younger than 3 Gyr in the LMC.

4.5 Evolution of the ISM

4.5.1 Star formation rate and stellar feedback

The LMC SFR is higher than the gas injection rate from SNe and AGB stars (in total 0.03–$0.07\,M_\odot\,\mathrm{yr}^{-1}$). Whitney et al. (2008) estimated a SFR of $0.19\,M_\odot\,\mathrm{yr}^{-1}$, and Kennicutt et al. (1995) suggested a SFR of $0.26\,M_\odot\,\mathrm{yr}^{-1}$. These are an order of magnitude higher than the gas output from AGB candidates and SNe. This suggests that the current LMC star formation depends on the large reservoir of ISM gas ($7 \times 10^8\,M_\odot$ in HI; Westerlund et al. (1997) and $1 \times 10^8\,M_\odot$ in H_2; Israel (1997)). This is summarised in Table 6. Without continuing infall, the LMC would become gas poorer, due to the excess SFR, and the SFR in the LMC would eventually decline. The Magellanic stream has in fact removed further material from the LMC. Further, stellar feed back for at least 1 Gyrs is required to gain 10% of gas mass present in the ISM, suggesting stellar yields can impact the ISM abundance only over a time scale of a few Gyrs. This is consistent with a time scale of the metallicity increases (order of a Gyr), according to the age-and-metallicity relation (e.g. Feast 1989; Russell & Dopita 1992; Pagel & Tautvaišienė 1998; Carrera et al. 2008).

4.5.2 Impact on extinction curve

The main sources of gas and dust are different in our Galaxy and in the LMC. This begs two questions: 1) why does the gas-to-dust ratio in the ISM in the LMC differ from that in the Galaxy? 2) Why do the proportions of amorphous silicate and carbon dust grains in AGB stars appear to differ from those in dust grains in the ISM.

The different enrichment may be expected to have an impact on the ISM. Gordon et al. (2003) measured that the gas-to-dust ratio varies within the LMC.

The highest values was found in the LMC 'supershell' ($\mathrm{N(HI)}/A(V)=5$–$23\times10^{21}\,\mathrm{atoms\,cm}^{-2}\,\mathrm{mag}^{-1}$), but overall gas-to-dust ratio remains similar ($\mathrm{N(HI)}/A(V)=1$–$7\times10^{21}\,\mathrm{atoms\,cm}^{-2}\,\mathrm{mag}^{-1}$) but slightly higher than the Galacitic value ($\mathrm{N(HI)}/A(V)=1.5\times10^{21}\,\mathrm{atoms\,cm}^{-2}\,\mathrm{mag}^{-1}$). Gordon et al. (2003) explained the variation with the local condition. The LMC 'supershell' is strongly affected by SNe, destroying dust grains.

The extinction curve in the LMC is quite similar to the Galactic one, except for a slight steep rise in far-UV region in 30 Dor region (Gordon et al. 2003). The 2175 Å bump is assumed to be associated with carbonaceous dust grains; this feature is weak in the 30 Dor region. Although the LMC has a higher carbonaceous dust input for AGB stars, compared to silicate dust, than does our Galaxy, this does not appear in the extinction curve. As Gordon et al. (2003) suggested, the extinction curve in 30 Dor region is strongly affected by SN dust destruction. However, overall the consistency of the extinction curve in the LMC and our Galaxy can not be explained with SN dust destruction. An additional silicate dust source may be required.

4.5.3 AGB feedback with respect to past SFR in the LMC and our Galaxy

We can estimate the gas and dust feedback rate from carbon-rich AGB stars and compare it with the mass removed from the ISM by star formation. We adopt the SFR in the bar and the disk from Smecker-Hane et al. (2002) of $0.01\,M_\odot\,\mathrm{yr}^{-1}\,\mathrm{deg}^{-2}$ and $0.004\,M_\odot\,\mathrm{yr}^{-1}\,\mathrm{deg}^{-2}$, respectively. These numbers approximately trace the SFR 1–3 Gyr ago, when most carbon-rich AGB stars were formed. The gas ejection rate ($\mathrm{GER_{cAGB}}$) and dust ejection rate ($\mathrm{DER_{cAGB}}$) from carbon-rich AGB stars are taken from Table 3. In the bar area, $\mathrm{GER_{cAGB}}/\mathrm{SFR}$ is 0.03–0.04 (up to 0.04) in mass, and outside of the bar the ratio is 0.02, i.e., the two regions have similar rates. This ratio could depend on the IMF, but no apparent difference is found in these two $\mathrm{GER_{cAGB}}/\mathrm{SFR}$. In the LMC, more high mass-loss rate AGB stars tend to be carbon-rich than oxygen-rich.

If we include the oxygen-rich stars, $\mathrm{GER_{AGB}}/\mathrm{SFR}$ could be higher than $\mathrm{GER_{cAGB}}/\mathrm{SFR}$ by a factor of 1.4–2, resulting in $\mathrm{GER_{AGB}}/\mathrm{SFR}$ of 0.03–0.08. If the SFR is approximately constant over the life time of the AGB stars, about 3–8 % of the stellar mass is returned to the ISM as gas through AGB stars. The uncertainties do not include the effect of the unknown condensation temperature of carbon-rich dust grains, which results in a systematic error of up to a factor of two on the colour and mass-loss rate relation. The ratio of the dust ejection rate from carbon-rich AGB stars to the SFR is 1–2×10^{-4}.

Similarly, we estimate the ratio of the gas ejection rate from AGB stars ($\mathrm{GER_{AGB}}$) to the SFR for Galactic stars, where we obtain 0.02–0.06 for $\mathrm{GER_{AGB}}/\mathrm{SFR}$ and 0.8–3×10^{-4}. Here we adopt the integrated AGB mass-loss rate of 3–$6\times10^{-4}\,M_\odot\,\mathrm{yr}^{-1}\,\mathrm{kpc}^{-2}$ (Jura & Kleinmann 1989). In

Table 6. Evolution of the ISM

Gas budget	
Stellar feedback (AGB + SNe)	$0.03 - 0.07 \, M_\odot \, \text{yr}^{-1}$
Star formation rate (SFR)	$0.19 - 0.26 \, M_\odot \, \text{yr}^{-1}$
Gas consumption rate (AGB + SNe − SFR)	$-0.23 - -0.12 \, M_\odot \, \text{yr}^{-1}$
Existing gas in the ISM (HI + H$_2$)	$8 \times 10^8 \, M_\odot$
Time to exhaust ISM gas	$\sim 3 \times 10^9$ years
Dust budget	
AGB dust production rate	$(5.5\text{–}11.5) \times 10^{-5} \, M_\odot \, \text{yr}^{-1}$
SNe dust production rate	$(0.01\text{–}13) \times 10^{-5} \, M_\odot \, \text{yr}^{-1}$
SNe dust destruction rate	?
Life time of dust	$2\text{–}4 \times 10^8$ years
Accumulated dust mass over the life time of dust (with constant rate)	$5 \times 10^4 \, M_\odot$
Existing dust in the ISM	$1.6 \times 10^6 \, M_\odot$
Age of the LMC	10–15 Gyrs

this case the sample is not limited to carbon-rich stars, as oxygen-rich stars are included. The SFR of our Galaxy is very uncertain and we adopt the value from Rana (1991), who suggest 0.01–$0.02 \, M_\odot \, \text{yr}^{-1} \, \text{kpc}^{-2}$ at 3 Gyrs ago. The measured AGB feedback rates in the LMC and the Galaxy are similar.

The AGB feedback rate can be compared with theoretical estimates. Stars within the mass range 1.0–$8.0 \, M_\odot$ comprise about 24 percent of the total mass of stars, according to Kroupa (2001). If these low- and intermediate-mass stars lose about 50–80 percent of their mass during the AGB phase, as estimated from the white dwarf mass, then 12–19 percent of the feedback to the ISM should theoretically be from these stars. The AGB feedback rate is only 3–8 percent of the stellar mass, with a potential increase up to 16 percent. In general, our observations are consistent with stellar feedback through AGB stars but it appears that the theoretical stellar feedback is slightly higher than the observed one.

4.5.4 Missing dust-source problem

The total dust mass in the ISM is approximately $1.6 \times 10^6 \, M_\odot$. For this estimate, we use the total ISM gas mass in the LMC of $8 \times 10^8 \, M_\odot$, and assume that the dust to gas extinction ratio in the LMC is about a factor of 2–2.5 lower than the Milky Way (Gordon et al. 2003; Cox et al. 2006), the adopted gas-to-dust ratio, of 500 in the LMC, is higher than the Galactic value (Zubko et al. 2004).

The total dust injection rate from carbon stars is measured to be $4.3 \times 10^{-5} \, M_\odot \, \text{yr}^{-1}$ and up to $1.0 \times 10^{-4} \, M_\odot \, \text{yr}^{-1}$. The rate from oxygen-rich stars is expected to be $1.2 \times 10^{-5} \, M_\odot \, \text{yr}^{-1}$. This is summarised in Table 6. Ignoring dust destruction, the dust mass in the ISM corresponds to about 20 Gyrs at the current injection rate, which is far too long. In fact, the life time of dust grains is of the order of 2–4×10^8 years, due to destruction by SN shocks (Jones et al. 1994), rather less than 20 Gyrs. Even adopting the highest dust production rate from SNe, the existing dust mass ($8 \times 10^8 \, M_\odot$) in the ISM is an order of magnitude high than the ex-

pected dust mass ($5 \times 10^4 \, M_\odot$) over constant dust supply from SNe and AGB stars over 4×10^8 years. This shows a 'missing dust-source problem' in the LMC.

A similar missing dust source problem is also found in high-z galaxies (Hughes et al. 1998; Morgan & Edmunds 2003). (Meikle et al. 2007) found that the total dust produced from SNe should be far less than the dust detected in the high-z galaxies (e.g. $10^8 \, M_\odot$; Bertoldi et al. 2003). Recently Sloan et al. (2009) found that AGB stars can contribute to dust production in addition to SNe, even for galaxies at z∼6. But although the dust production AGB stars can alleviate the discrepancy, it is unlikely to resolve it in high-z galaxies. Additional dust sources are therefore needed in the ISM in both the LMC and high-z galaxies. One possibility is star formation regions, as suggested by Morgan & Edmunds (2003). Alternatively, dust processing and dust growth by gas accretion in the ISM may yield a total dust mass in the ISM which exceeds the dust mass produced by stars.

5   CONCLUSIONS

We have analysed Spitzer data for AGB stars in the LMC, and presented a quantitative analysis of gas and dust budge in the LMC ISM. We obtain the following main conclusions:

- The mass-loss rates of the AGB stars are a quantifiable function of their infrared colours.
- The total mass-loss rate from all carbon-rich AGB candidates is estimated to be $8.6 \times 10^{-3} \, M_\odot \, \text{yr}^{-1}$ (up to $21 \times 10^{-3} \, M_\odot \, \text{yr}^{-1}$) in gas and $4.3 \times 10^{-5} \, M_\odot \, \text{yr}^{-1}$ (up to $1 \times 10^{-4} \, M_\odot \, \text{yr}^{-1}$) in dust in the LMC. Adding oxygen-rich AGB stars could increase the gas feedback rate to $15 \times 10^{-3} \, M_\odot \, \text{yr}^{-1}$ (up to $27 \times 10^{-3} \, M_\odot \, \text{yr}^{-1}$) and the dust feedback rate to $6 \times 10^{-5} \, M_\odot \, \text{yr}^{-1}$ (up to $1 \times 10^{-4} \, M_\odot \, \text{yr}^{-1}$) from AGB stars.
- AGB stars are among the main sources of gas and dust in the LMC. AGB stars are the dominant source of gas in the disc, but SNe are a slightly more important gas source in the bar region of the LMC. The gas injection rate from SNe could be as high as $4 \times 10^{-2} \, M_\odot \, \text{yr}^{-1}$

in the LMC, but the dust production of SNe is uncertain.

• The measured feedback from carbon-rich AGB stars into the ISM is 2–4 percent of the SFR 3 Gyr ago for gas mass, and 0.01–0.02 percent of the SFR for dust mass. The gas feedback from both carbon-rich and oxygen-rich AGB stars is expected to be 3–8 percent of the SFR. These values could increase by a factor of two, due to the uncertainty of dust condensation temperature. These ratios appear to be similar in number within the LMC bar, the disk and Galactic disk.

• The gas output of SNe is found to be more important in the LMC bar than in both the remaining region of the LMC and in the Galaxy, related to a higher gas-to-dust ratio in the LMC.

• The total gas mass supplied through AGB stars and SNe is far less than the current star formation rate. The star formation largely depends on the gas already present in the LMC ISM, and without infall, eventually the SFR will decline as a consequence of the gas exhaustion in the ISM.

• In the LMC, there is 'a missing dust source' problem present. The largest estimate of dust accumulation from AGB stars and SNe can not account for the full dust mass in the ISM. This is a similar problem as found for high-z galaxies. Additional dust sources are required, possibly located in star-forming regions.

6 ACKNOWLEDGMENTS

REFERENCES

Aoki W., Tsuji T., Ohnaka K., 1998, A&A 340, 222

Bastian N., Gieles M., Ercolano B., Gutermuth R., 2009, MNRAS 392, 868

Battinelli P., Demers S., Mannucci F., 2007, A&A 474, 35

Bekki K., Chiba M., 2005, MNRAS 356, 680

Bernard-Salas J., et al., submitted to ApJ

Bertoldi F., Carilli C.L, Cox P., et al., 2003, A&A 406, L55

Blanco B.M., Blanco V.M., McCarthy M.F., 1978, Nature, 271, 638

Blanco V.M., Mc Carthy M.F., 1983, AJ 88, 1442

Blanco V.M., Blanco B.M., McCarthy M.F., 1980, ApJ 242, 938

Blum R.D., et al., 2006, AJ 132, 2034

Bohlin R.C., Savage B.D., Drake J.F., 1978, ApJ 224, 132

Bolatto A.D., et al., 2007, ApJ 655, 212

Boothroyd A.I., Sackmann I.-J., Ahern S.C., 1993, ApJ 416, 762

Bot C., Boulanger F., Lagache G., Cambrésy L., Egret D., 2004, A&A 423, 567

Bowen G.H., Willson L.A., 1991, ApJ 375, L53

Breysacher J., Azzopardi M., Testor G., 1999, A&AS 137, 117

Buchanan C.L., Kastner J.H., Forrest W.J., Hrivnak B.J., Sahai R., Egan M., Frank A., Barnbaum C., 2006, AJ 132, 1890

Carrera R., Gallart C., Hardy E., Aparicio A., & Zinn R., 2008, AJ, 135, 836

Chen P.S., Kwok S., 1993, ApJ 416, 769

Chiappini C., Matteucci F., Romano D. 2001, ApJ, 554, 1044

Cioni M.-R.L., Girardi L., Marigo P., Habing H.J., 2006a, A&A 448, 77

Cioni M.-R.L., Girardi L., Marigo P., Habing H.J., 2006b, A&A 452, 195

Cioni M.-R.L., Habing H.J., 2003, A&A 402, 133

Cioni M.-R.L., Habing H.J., Israel F.P., 2000a, A&A 358, L9

Cioni M.-R.L., Marquette J.-B., Loup C., Azzopardi M., Habing H.J., Lasserre T., Lesquoy E., 2001, A&A 377, 945

Cioni M., van der Marel R., Loup C., Habing H., 2000b, A&A 359, 601

Cioni M.-R. L., Bekki K., Clementini G., et al. 2008, PASA 25, 121

Clayton G.C, Green J.W., Michael J.Z., Nicolle E.B., Code A.D., Davidsen A.F., 1996, ApJ 460, 313

Condon J.J., 1992, ARA&A 30, 575

Cox N.L.J., Cordiner M.A., Cami J., Foing B.H., Sarre P.J., Kaper L., Ehrenfreund P., 2006, A&A 447, 991

Crowther P.A., Smith L.J., 1997, A&A 320, 500

Dopita M.A., Vassiliadis E., Wood P.R., et al., 1997, ApJ 474, 188

Dwek E., 1998, ApJ 501, 643

Dwek E., et al., 2008, ApJ 676, 1029

Egan M.P., Van Dyk S.D., Price S.D., 2001, AJ, 122, 1844

Elson R.W., Gilmore G.F., Santiago B.X., 1997, MNRAS, 289, 157

Ercolano B., Barlow M.J., Sugerman B.E.K., 2007, MNRAS 375, 753

Evans C.J., Crowther P.A., Fullerton A.W., Hillier D.J., 2004, ApJ 610, 1021

Fazio G.G., et al., 2004, ApJS 154, 10

Feast M.W., 1989, IAU Colq. 111, Cambridge and New York, Cambridge University Press, 1989, p. 205

Feast M.W., 1995, Proceedings of IAU Symp. 164, 'Stellar populations', p153

Feast M.W., Whitelock P.A., Menzies J.W., 2006, MNRAS 369, 791

Filipović M.D., et al., 1998, A&AS 127, 119

Finlator K., Davé R., 2008, MNRAS, 385, 2181

Fitzpatrick E.L., 1985, ApJ 299, 219

Gehrz R., 1989, in Allamandola L.J., Tielens A.G.G.M., eds, Proceedings of IAU Symp. 135, 'Interstellar Dust', p. 445

Glass I.S., et al., 1999, MNRAS 308, 127

Gordon K.D., Clayton G.C, Misselt K.A, Landolt A.U., Wolff M.J., 2003, ApJ 594, 279

Gordon K.D., Clayton G.C., 1998, ApJ 500, 816

Gouliermis D.A., Quanz S.P., Henning Th., 2007, ApJ 665, 306

Groenewegen M.A.T., de Jong T., Gaballe T.R., 1994, A&A 287, 163

Groenewegen M.A.T., Whitelock P.A., Smith C.H., Kerschbaum F., 1998, MNRAS 293, 18

Groenewegen M.A.T., 2006, A&A 448, 181

Groenewegen M.A.T., 2007, 'Why Galaxies Care About AGB Stars: Their Importance as Actors and Probes', ASP Conference Series 378, p 433

Groenewegen M.A.T., de Jong T., van der Bliek N.S., Slijkhuis S., Willems F.J., 1992, A&A 253, 150

Groenewegen M.A.T., et al., 2007, MNRAS 376, 313

Gruendl R.A., Chu Y.-H., Seale J.P., Matsuura M., Speck A.K., Sloan G.C., Looney L.W., 2008, ApJ 688, L9

Habing H.J., 1996, A&ARv 7, 97

Hillier D.J., Davidson K., Ishibashi K., Gull T., 2001, ApJ 553, 837

Hirashita H., Ferrara A., 2002, MNRAS 337, 921

Houck J.R., et al., 2004, ApJS 154, 18

Hora J.L., et al., 2008, AJ 135, 725

Hughes D.H, Serjeant S., Dunlop J., et al., 1998, Nature 394, 241

Hughes S.M.G., 1989, AJ 97, 1634

Hughes S.M.G., Wood P.R., 1990, AJ 99, 784

Israel F.P., 1997, A&A 328, 471

Ita Y., et al., 2008, PASJ, 60, S435

Ivezić Z., Elitzur M., 1995, ApJ 445, 415

Izumiura H., Hashimoto O., Kawara K., Yamamura I., Waters L.B.F.M., 1996, A&A 315, L221

Jones A.P., Tielens A.G.G.M., Hollenbach D.J., McKee C.F., 1994, ApJ 433, 797

Jones A.P., Tielens A.G.G.M., Hollenbach D.J., 1996, ApJ 469, 740

Jørgensen U.G., Hron J., Loidl R., 2000, A&A 356, 253

Jura M., 1987, ApJ 313, 743

Jura M., 1994, ApJ 422, 102

Jura M., Kleinmann S.G., 1990, ApJ 364, 663

Jura M., Kleinmann S.G., 1989, 341, 359

Karakas A., Lattanzio J.C., 2007, PASA 24, 103

Kastner J.H., Thorndike S.L., Romanczyk P.A., Buchanan C., Hrivnak B.J., Sahai R., Egan M., 2008, AJ 136, 1221

Kato D., et al., 2007, PASJ 59, 615

Keller S.C., Wood P.R., 2006, ApJ 642, 834

Kennicutt R.C, Bresolin F., B., Bomans D.J., Bothun G.D., Thompson I.B., 1995, AJ 109, 594

Knapp G.R., Morris M., 1985, ApJ 292, 640

Kodama T., Arimoto N., 1997, A&A 320, 41

Kontizas E., Dapergolas A., Morgan D.H., Kontizas M., 2001, A&A 369, 932

Koornneef J., 1982, A&A, 107, 247

Kroupa P., 2001, MNRAS 322, 231

Kraemer K.E., Sloan G.C., Bernard-Salas J., Price S.D., Egan M.P., Wood P.R., 2006, ApJ 652, L25

Lagadec E., et al., 2007, MNRAS 376, 1270

Lagadec E., Zijlstra A.A., 2008a, MNRAS, 390, L59

Lagadec E., et al., 2008b, MNRAS 383, 399

Lançon A., Wood P.R., 2000, A&AS 146, 217

Leão I.C., De Laverny P., Mékarnia D., de Medeiros J.R., Vandame B., 2006, A&A 455, 187

Le Bertre T., 1992, A&AS 94, 377

Le Bertre T., 1997, A&A 324, 1059

Le Bertre T., Matsuura M., Winters J.M., Murakami H., Yamamura I., Freund M., Tanaka M., 2001, A&A 376, 997

Le Bertre T., Winters J.M., 1998, A&A 334, 173

Leisenring J.M., Kemper F., Sloan G.C., 2008, ApJ 681, 1557

Leisy P., Dennefeld M., 1996, A&AS 116, 95

Little-Marenin I.R., Little S.J., 1988, ApJ 333, 305

Lodders K., Fegley B., 1995 Meteoritics, 30, 661

Maeder, A., 1992, A&A, 264, 105

Marigo P., 2007, A&A 467, 1139

Marigo P., Girardi L., 2007, A&A 469, 239

Marigo P., Girardi L., Bressan A., Groenewegen M.A.T., Silva L., Granato G.L., 2008, A&A 482, 883

Marshall J.R., van Loon J.Th., Matsuura M., Wood P.R., Zijlstra A.A., Whitelock P.A. 2004, MNRAS 355, 1348

Mathewson D.S., Ford V.L., Dopita M.A., Tuohy I.R., Long K.S., Helfand D.J., 1983, ApJS 51, 345

Matsuura M., Yamamura I., Cami J., Onaka T., Murakami H., 2002a, A&A 383, 972

Matsuura M., Zijlstra A.A., van Loon J.Th., Yamamura I., Markwick A.J., Woods P.M., Waters L.B.F.M., 2002b, ApJ 580, L133

Matsuura M., et al., 2005 A&A 434, 691

Matsuura M., et al., 2006, MNRAS 371, 415

Matsuura M., et al., 2007, MNRAS, 382, 1889

Mattsson L., Wahlin R., Höfner S., Eriksson K., 2008, A&A 484, L5

Meikle W.P.S., Mattila S., Pastorello A., et al., 2007, ApJ 665, 608

Meixner M., et al., 2006, AJ 132, 2268

Misselt K.A., Clayton G.C, Gordon K.D., 1999, ApJ 515, 128

Moffat A.F.J., 1991, A&A 244, L9

Morgan H.L., Edmunds M.G., 2003, MNRAS 343, 427

Moseley S.H., Dwek E., Glaccum W., Graham J.R., Loewenstein R.F., 1989, Natur 340, 697

Murakami H., et al., 2007, PASJ 59, S369

Nakamura T., Umeda H., Nomoto K., Thielemann F., Burrows A., 1999, ApJ 517, 193

Nikolaev S., Weinberg M.D., 2000, ApJ 542, 804

Ohnaka K., Driebe T., Hofmann K.-H., Weigelt G., Wittkowski M., 2008, A&A 484, 371

Ojha D.K., Tej A., Schultheis M., Omont A., Schuller F., 2007, MNRAS 381, 1219

Pagel B.E.J., Tautvaišienė G., 1998, MNRAS 299, 535

Reid N., Glass I.S., Catchpole R.M., 1988, MNRAS 232, 53

Reid W.A., Parker Q.A., 2006, MNRAS 373, 521

Rana N.C., 1991, ARA&A 29, 129

Rho J., et al., 2008, ApJ, 673, 271

Rieke G.H., et al. 2004, ApJS 154, 25

Ridgway S.T., Carbon D.F., Hall D.N.B., 1978, ApJ 225, 138

Russell S.C., Dopita M.A., 1992, ApJ 384, 508

Sakon I., et al., 2008, submitted to ApJ (astro-ph/07114801)

Salpeter E.E., 1955, ApJ 121, 161

Sanduleak N., Philip A.G.D., 1977, PASP 89, 792

Schwering P.B.W., Israel, F.P., 1990, 'Atlas and catalogue of infrared sources in the Magellanic Clouds', Kluwer, Dordrecht

Sloan G.C., et al., 2006, ApJ 645, 1118

Sloan G.C., Kraemer K.E., Wood P.R., Zijlstra A.A., Bernard-Salas J., Devostand D., Houck J.R., 2008, ApJ, 686, 1056

Sloan G.C., Matsuura M., Zijlstra A.A., et al., 2009, Science, 323, 353

Skinner C.J., Justtanont K., Tielens A.G.G.M., Betz A.L., Boreiko R.T., Baas F., 1999, MNRAS 302, 293

Skrutskie M.F, et al., 2006, AJ 131, 1163

Smartt S.J., Eldridge J.J., Crockett R.M., Maund, J.R., 2008, MNRAS accepted, (arXiv/0809.0403)

Smecker-Hane T.A., Cole A.A., Gallagher J.S. III, Stetson P.B., 2002, ApJ 566, 239

Smith L.F., 1988, ApJ 327, 128

Speck A.K., et al. 2006, ApJ 650, 892

Srinivasan S., et al., 2008, submitted to ApJ

Stancliffe R.J, Izzard R.G., Tout C.A., 2005, MNRAS 356, L1

Stanghellini L., Shaw R.A., Gilmore D., 2005, ApJ 622, 294

Stanimirović S., 2005, ApJ 632, L103

Stanghellini L., Garcia-Lario P., Garcia-Hernandez D.A., Perea-Calderon J.V., Davies J.E., Manchado A., Villaver E., Shaw R.A., 2007, ApJ 671, 1669

Sugerman B.E.K., et al., 2006, Sci 313, 196

Tanabé T., Nishida S., Matsumoto S., Onaka T., Nakada Y., Soyano T., Ono T., Sekiguchi K., Glass I. S., 1997, Nature 385, 509

Tej A., Lançon A., Scholz M., Wood P.R., 2003, A&A 412, 481

Thronson H.A., Jr., Latter W.B., Black J.H., Bally J., Hacking P., 1987, ApJ 322, 770

Tielens A.G.G.M., 1990, CGSE, NASA p59

Tielens A.G.G.M., McKee C.F., Seab C.G., Hollenbach D.J., 1994, ApJ 431, 321

Tielens A.G.G.M., Waters L.B.F.M., Bernatowicz T.J., 2005, ASPC 341, 605

Tonini C., Maraston C., Devriendt J., Thomas D., Silk J., 2008, MNRAS submitted (arXiv0812.1225)

Tsuji T., Ohnaka K., Aoki W., Yamamura I., 1997, A&A 320, L1

Tsujimoto T., Nomoto K., Yoshii Y., Hashimoto M., Yanagida S., Thielemann F.-K., 1995, MNRAS 277, 945

van Boekel R., Waters L.B.F.M., Dominik C., Bouwman J., de Koter A., Dullemond C.P., Paresce F., 2003, A&A 400, L21

van der Veen W.E.C.J., Habing H.J., 1988, A&A 194, 125

Van Genderen A.M., 2001, A&A 366, 508

van Loon J.Th., 2000, A&A 354, 125

van Loon J.Th., Groenewegen M.A.T., De Koter A., Trams N.R., Waters L.B.F.M., Zijlstra A.A., Whitelock P.A., Loup C., 1999, A&A 351, 559

van Loon J.Th., Cioni M.-R. L., Zijlstra A.A., Loup C., 2005, A&A 438, 273

Vassiliadis E., & Wood P.R., 1993, ApJ, 413, 641

Verhoelst T., Van der Zypen N., Hony S., Decin L., Cami J., Eriksson K., 2009, A&A in press (arXiv0901.1262)

Voors R.H.M., et al., 2000, A&A 356, 501

Wachter A., Winters J.M., Schröder K.-P., Sedlmayr E., 2008, A&A, 486, 497

Weingartner J.C., Draine B.T., 2001, ApJ 548, 296

Werner M.W., et al., 2004, ApJS 154, 1

Westerlund B.E., 1997, 'The Magellanic Clouds', Cambridge Univ. Press

Westerlund B.E., Azzopardi M., Rebeirot E., Breysacher J., 1991, A&AS 91, 425

Westerlund B.E., Olander N., Hedin B., 1981, A&AS 43, 267

Whitelock P.A., Catchpole R.M., 1987, MNRAS 212, 873

Whitelock P.A., et al., 1989, MNRAS 240, 7

Whitelock P., Menzies J., Feast M., Marang F., Carter B., Roberts G., Catchpole R., Chapman J., 1994, MNRAS 267, 711

Whitelock P.A., Feast M.W., Marang F., Groenewegen M.A.T., 2006, MNRAS 369, 751

Williams R.M., Chu, Y.-H., Dickel, J.R, Petre R., Smith R.C., Tavarez M., 1999, ApJS 123, 467

Whitney B.A, et al., 2008, AJ 136, 18

Wood P.R., Bessell M.S., Fox M.W., 1983, ApJ 272, 99

Wood P.R., Bessell M.S., Paltoglou G., 1985, MNRAS 290, 477

Wood P.R., Cohen M., 2001, in R. Szczerba R., Górny S.K., eds., Astrophysics and Space Science Library Vol. 265, Post-AGB objects as a phase of stellar evolution, Kluwer Academic Publishers, Boston/Dordrecht/London, p. 71

Wood P.R., Whiteoak J.B., Hughes S.M.G., Bessell M.S., Gardner F.F., Hyland A.R., 1992, ApJ 397, 552

Wood P.R., Habing H.J., McGregor P.J., 1998, A&A 336, 925

Wood P.R., Groenewegen M.A.T., Sloan G.C., Blommaert J.A.D.L., Cioni M.-R.L., Feast M.W., Habing H.J., Hony S., Lagadec E., 2007, ASPC 378, 251

Wright A.E., Barlow M.J., 1975, MNRAS 170, 41

Zaritsky D., 1999, AJ 118, 2824

Zhukovska S., Gail H.-P., Trieloff M., 2008, A&A 479, 453

Zickgraf F.-J., 2006, ASPC 355, 135

Zijlstra A.A., et al., 2006, MNRAS 370, 1961

Zijlstra, A. A., Bedding, T. R., & Mattei, J. A. 2002, MNRAS, 334, 498

Zubko V., Dwek E., Arendt R.G., 2004, ApJS 152, 211

Zuckerman B., Dyck H.M., 1989, A&A 209, 119

APPENDIX A: CLASSIFICATION OF CARBON-RICH STARS

A1 Existing classification schemes

Fig. A1 shows a $J - Ks$ vs Ks colour magnitude diagram for the LMC stars from the SAGE catalogue. The coding of the chemical types of the stars is given in the figure. There are five branches within $11 > Ks > 7$. Carbon-rich stars are found in the reddest of these branches ($J - Ks \gtrsim 1.4$), as is known from previous studies (Nikolaev & Weinberg 2000). From $J - Ks \sim 1.4$ to 2.0 mag there is a bend in the carbon-rich branch and the Ks-mag becomes brighter with colour. This branch reaches its brightest Ks-mag at about $J-Ks \sim 2$, after which Ks becomes fainter. The number density also decreases redward of $J - Ks \sim 2$. Stars with $J - Ks > 2$ are described as obscured AGB stars by Nikolaev & Weinberg (2000), and in our sample most of these are carbon-rich, but oxygen-rich stars are also found here. Following the classification by Cioni et al. (2006a) ($Ks < -0.48 \times (J - Ks) + 13$ and $Ks < -13.333 \times (J - Ks) + 24.666$), only 17 percent of the stars are redder than $J - Ks > 2$. This shows that less than one-sixth of carbon-stars have a circumstellar envelope detectable in the Ks-band. This is consistent with the stellar evolution model by Marigo et al. (2007), who showed that the super-wind phase (with mass-loss rate higher than $5.6 \times 10^{-7} M_\odot \, \mathrm{yr}^{-1}$) lasts less than 15 percent of the thermal-pulsing lifetime for carbon-stars.

The 2MASS sensitivity is not sufficiently high to detect dusty carbon-rich AGB stars in some bands. Figs. A2 and A3 show that 2MASS does not detect the J- and Ks-bands at the red end of the carbon-rich sequence. However, this red end is clearly detected at [5.8] and [8.0] (Fig. 4 and Fig. A4). The situation will change once the VISTA LMC survey of the Magellanic System is completed, which could detect as faint as Ks=20.3 mag (Cioni et al. 2008).

Oxygen-rich stars are mainly found at $Ks \sim 8$ mag and $J - Ks < 1.5$. These stars are a mixture of red giants and red-super giants (Kastner et al. 2008). Cioni & Habing (2003) show that oxygen-rich AGB stars are found in the branch located at about $Ks \sim 9$ mag and $J-Ks < 1.5$. In our analysis (Fig. A1), there are two regions with oxygen-rich stars. One is the same as identified by Cioni & Habing (2003). The other is occupied by oxygen-rich stars with think dust shell, which are just above the obscured carbon-rich sequence. There are two oxygen-rich stars with lower luminosity than the others ($Ks \sim 13$ mag; $J - Ks$=1.5–2.0): l63-31(SAGE 045433.86−692036.1) and MSX LMX 610. Their low luminosities and some excess at near-infrared wavelengths suggest that they could be oxygen-rich post-AGB candidates or YSO candidates. Post-AGB stars with optical variability show similar $J - Ks$ and Ks-magnitudes (Wood & Cohen 2001). The possibility that they are YSOs is not discarded, but if so the $Ks \sim 13$ mag implies a relatively high mass (between 5 and 10 $M_\odot$; Whitney et al. 2008).

Fig. A2 shows the $J - [3.6]$ vs [3.6] colour magnitude diagram, used by Blum et al. (2006), in which the separation of oxygen- and carbon-
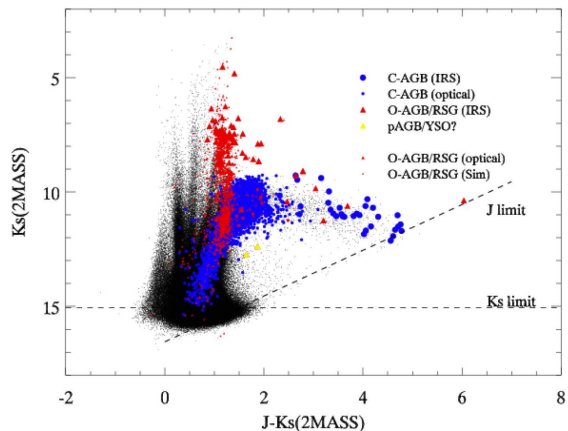

Figure A1. 2MASS $J-Ks$ vs Ks colour magnitude diagram for the LMC, extracted from the SAGE catalogue. The lower graph shows cross-identifications with carbon-rich AGB stars, oxygen-rich AGB stars and RSGs. Large blue circles: carbon-rich AGB stars according to their IRS spectra. Small blue circles: carbon-rich AGB stars from (Kontizas et al. 2001), classified from optical spectra. Red triangles: oxygen-rich red giants and supergiants based on IRS spectra.

rich AGB stars is clear. Oxygen-rich stars have OH in the J-band, and most Mira variables have H_2O in JHK- and L-bands (Lançon & Wood 2000; Tsuji et al. 1997; Matsuura et al. 2002a; Tej et al. 2003). Carbon-rich stars have HCN and C_2H_2 bands at $3.1 \, \mu m$ (Ridgway et al. 1978; Groenewegen 1994; van Loon et al. 1999; Matsuura et al. 2002b, 2005) and CN in the J- and H-bands (Whitelock & Catchpole 1987; Lançon & Wood 2000). The sensitivity is limited by the J-band, and heavily dust-obscured AGB stars are not detected. In Fig. A1 optically identified carbon stars listed by Kontizas et al. (2001) reach the brightest Ks mag. The Ks magnitudes become fainter as the stars become redder in $J - Ks$, as they do among the more obscured carbon stars classified by Spitzer IRS. In contrast, such a trend is not found in Fig. A2; the [3.6] magnitude continues to brighten among obscured carbon stars beyond the J-band detection limit, as would be expected.

A2 Classification using $Ks - [8.0]$ vs Ks

Fig. A3 is a colour-magnitude diagram showing $Ks - [8.0]$ vs Ks. In this carbon-rich stars become fainter in Ks as circumstellar reddening changes the colour; Ks reaches a peak of $Ks \sim 10$ mag around $Ks - [8.0] = 2$–4 mag. Oxygen-rich stars have slightly higher luminosity in Ks at a given colour, except for the two oxygen-rich post-AGB/YSO candidates. In this diagram, oxygen-rich stars are well separated from carbon-rich stars. LMC carbon-rich stars have HCN and C_2H_2 absorption bands at $7 \, \mu m$ (Aoki et al. 1998; Jørgensen et al. 2000; Matsuura et al. 2006) in the [8.0]-band (6.5–9.5 μm) while oxygen-rich stars have only weak SiO absorption and silicate excess in the [8.0]-band, until the sil-
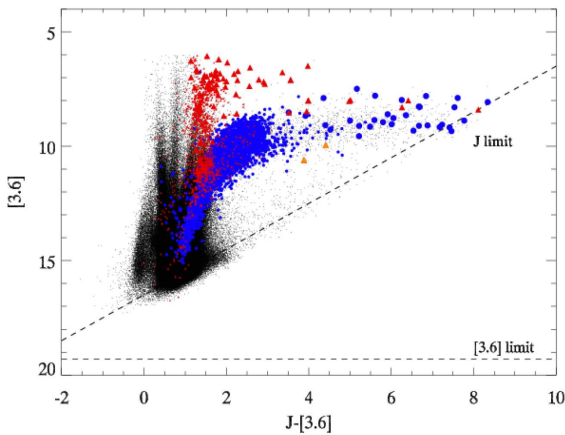
Figure A2. J-band and $J - [3.6]$ colour magnitude diagram.

icate band turns to absorption. These spectral differences separate the two chemical types in this colour-magnitude diagram. This diagram also shows that high mass-loss rate carbon-rich stars could have Ks-band magnitudes fainter than 15 mag, i.e., below the detection limit of the 2MASS Ks-band.

A3   Other colour-magnitude diagrams

High mass-loss rate stars are likely to be detected at longer wavelength, as is illustrated in the Spitzer SAGE colour-magnitude diagrams discussed below. Figs. A4 and A5 show colour-magnitude diagrams using the SAGE [5.8]-, [8.0]- and [24]-bands. In these two figures the sequence of IRS-classified carbon-rich stars does not end at the detection limits. Thus all of the red, i.e., high mass-loss rate carbon-rich, stars were detected in these bands. However, there is no clear separation between oxygen-rich and carbon-rich stars so the diagrams are not useful for classification.

A4   Near-infrared survey with the IRSF

Kato et al. (2007) published a $JHKs$ survey of the Magellanic Clouds taken with the Infrared Survey Facility (IRSF) telescope at SAAO in South Africa. The sensitivity of this survey, 16.6 mag at $10\,\sigma$ in the Ks band for the LMC, is significantly better than that of 2MASS (14.3 mag), although the conversion between IRSF and 2MASS filter system may not be straightforward for AGB stars (Kato et al. 2007). Four of the stars listed in Groenewegen et al. (2007) have been observed with IRSF and their mass-loss rate is plotted in Fig. A6. It appears that IRSF stars follow a similar colour mass-loss rate trend. We will investigate this relation further after the Spitzer spectroscopic survey, SAGE-Spec, is complete.
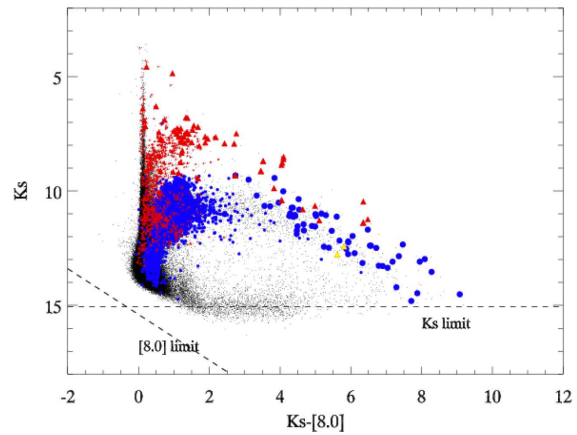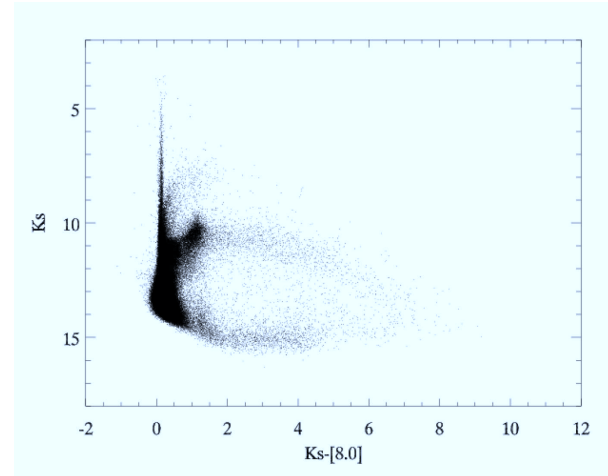

Figure A3. Ks and $Ks - [8.0]$ colour magnitude diagram. The upper panel shows all of the SAGE sample, and spectroscopically known oxygen-rich AGB/RSGs, while carbon-rich AGB stars are indicated in the lower panel. The Ks-band sets the detection limit at $Ks - [8.0] < 2$ mag, except for blue ($Ks - [8.0] < 2$ mag) stars, which are [8.0]-band limited. The number of carbon-rich AGB stars decreases at about $Ks - [8.0]=1.4$
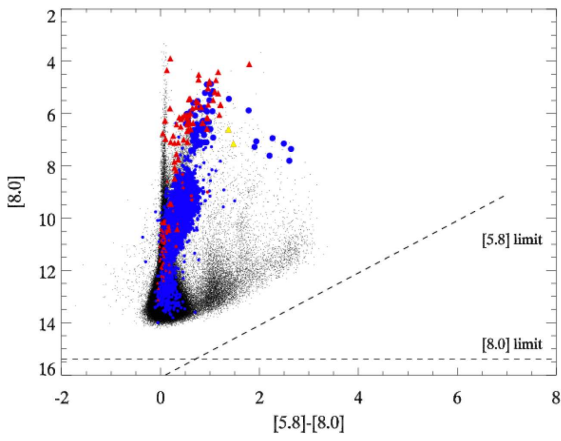
Figure A4. $[5.8]-[8.0]$ vs $[8.0]$ colour-magnitude diagram. Symbols are the same as in Fig.A1. Oxygen-rich and carbon-rich stars are found close together.
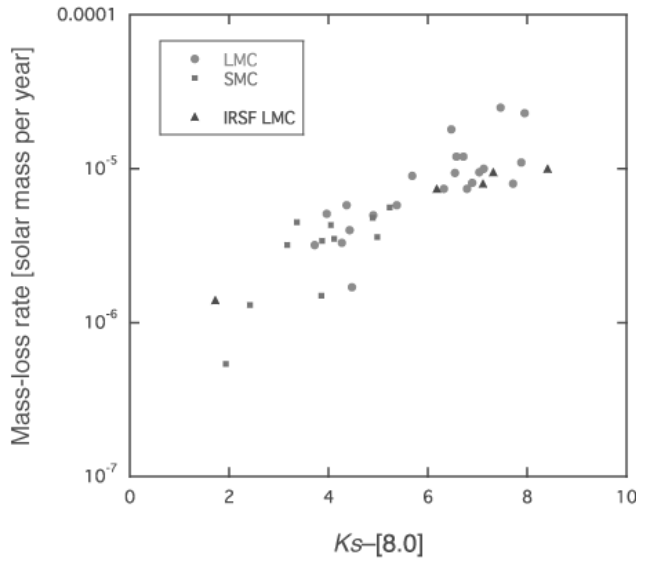

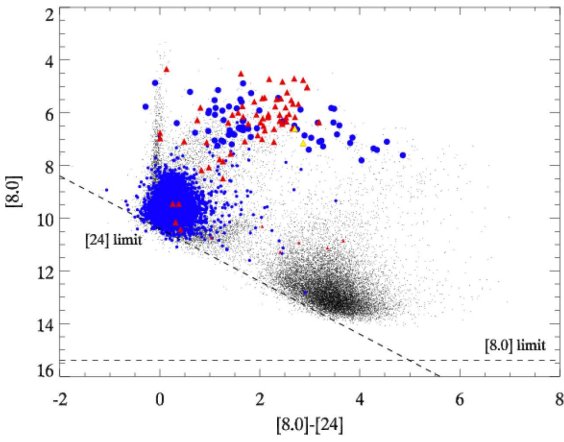**Figure A6.** The $Ks-[8.0]$ using IRSF Ks is plotted

Figure A5. $[8.0]-[24]$ vs $[8.0]$ colour-magnitude diagram. Symbols are the same as Fig.A1. Oxygen-rich and carbon-rich stars are not separated.
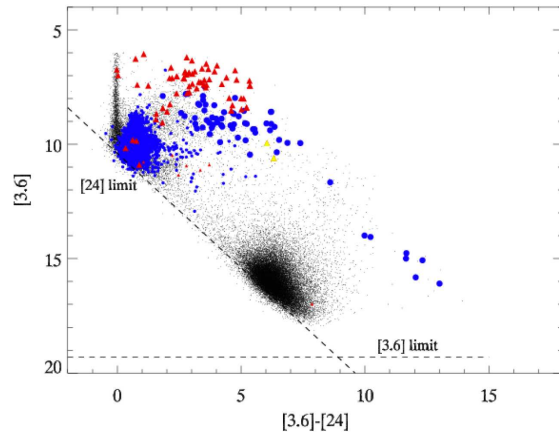

Figure A7. $[3.6]-[24]$ vs $[24]$ colour-magnitude diagram. Symbols are the same as A1.